Transfer Report

January 2017

Naomi Omori

Supervised by Professor Andrew Beale

Department of Chemistry, UCL

Table of Contents

1 Research Question

As scientific understanding of catalytic systems advances, so too does the need for characterisation techniques that provide more specific and localised catalytic information. In an ideal world, obtaining the most catalytically relevant information would begin with access to a real-time view of one's sample with both infinitely refined temporal and spatial resolution. It is not difficult to imagine the novelty of a technique that could offer, for example, quantitative images with nanoscale resolution depicting the spatial distribution of catalytically active sites across a sample.

Optical microscopy, utilised widely in the biological sciences, has become increasingly sophisticated, with Nobel prize-worthy improvements in resolution and flexible commercial systems capable of imaging multiple modalities simultaneously. While not currently a staple of the catalytic chemist's characterisation arsenal, it is possible that state-of-the-art optical microscopy techniques could provide a new window into how and why catalysts function the way that they do.

This project aims to assess the suitability of novel and advanced optical imaging techniques for the characterisation of catalytic materials. A particular focus will be placed on microscopy techniques that can be performed *in situ* and yield super-resolution images. It is hypothesised that fluorescence and super-resolution imaging of catalysts will be possible, and it is hoped that fluorescence images with a level of detail on par with electron microscope techniques.

Work to date indicates that a wide range of catalytically relevant samples can be imaged using optical fluorescence microscopy. Future work will be focused more on optimising microscope configurations and acquisition parameters to obtain quantifiable images. With quantifiable images, it is hoped that more specific information such as identifying particular hydrocarbon species in a zeolite may become possible.

2 Methodology

2.1 Theoretical Background

Fluorescence is a process whereby specific molecules, termed fluorophores, emit photons following absorption of incident electromagnetic radiation. The fluorescence process can be conceptually separated into three stages, each of which operates on timescales differing by several orders of magnitude.

2.1.1 The Excited State

Fluorescence begins when a fluorophore is excited into a higher energy state via a rapid femtosecond process called photoexcitation. In photoexcitation, an electron absorbs the full energy of a photon, elevating the electron to a higher-energy typically antibonding orbital. A classical visualisation of transitions through molecular energy levels is best summarised in a Jablonski diagram, presented below in Figure 1. Here, thick lines represent singlet and triplet electronic energy levels, and thinner lines represent vibrational energy states.

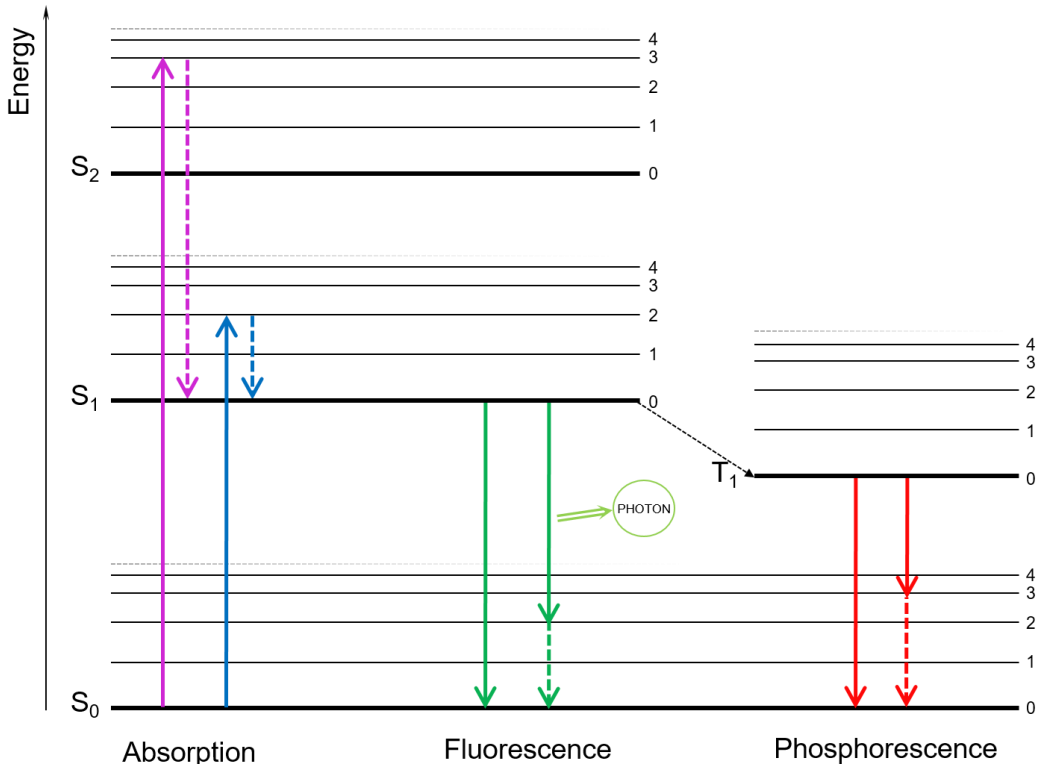

Figure 1 Jablonski diagram of fluorophore excitation where S_0 is the ground singlet electronic state, S_1 and S_2 are higher energy singlet states, and T_1 is the lowest possible triplet state. Rotational states have not been included.

Ground and excited energy states where electron spins are paired are called singlet states (S_0, S_1, etc.), and have a spin of 0. As shown in Figure 2, when electrons are promoted

from a ground singlet to an excited singlet state, the paired spin orientation is maintained. Excited states where unpaired electrons are present are termed triplet states (T_1, T_2, etc.), and have a spin of 1. In other words, unpaired electrons in the excited triplet state will have the same spin orientation to the other unpaired electron. The vast majority of compounds exist with singlet ground states, although examples of triplet ground states such as dioxygen do exist.

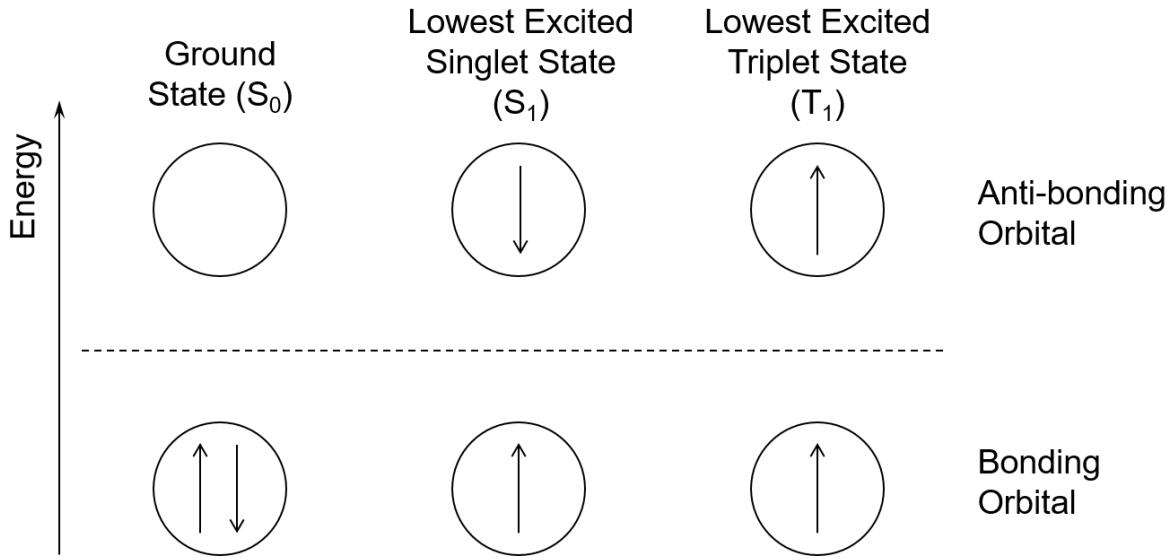

Figure 2 Diagrammatic representation of electronic configurations in the ground and excited states of a diatomic molecule with two σ electrons

The left of Figure 1 demonstrates two arbitrary examples of absorption pathways. Given that energy states are discretely quantised, absorption will only occur for particular wavelengths carrying specific energies correlating to particular band gaps between the fluorophore's ground and excited states. This concept is not as limiting as it may at first seem, as it can be inferred from Figure 1 that more complex fluorophores will have a larger number of electronic and vibrational states capable of being excited. Consider Planck's Law for energy in a quantum, where energy is inversely proportional to the wavelength of radiation:

$$E = \frac{hc}{\lambda}$$

Where h = Planck's constant

c = speed of light

λ = wavelength

Energy of different wavelengths therefore spans across a spectrum, with a shift towards higher energies as light tends towards the UV region. Figure 1 demonstrates that UV light is not only more strongly absorbing, but different wavelengths are capable of exciting the

fluorophore to different energy states. The result is that complex molecules will have broader absorption spectra than a simple molecular system.

2.1.2 Decay Pathways

Excited molecules may return to the ground state through a combination of different decay processes. Radiative decay is molecular de-excitation accompanied by photon emission. Non-radiative decay is molecular de-excitation without photon emission. In the case of fluorescence, decay can be either radiative or a combination of radiative and non-radiative pathways as demonstrated in Figure 1 where non-radiative internal conversion, represented as a dashed line, forms part of the radiative fluorescence emission.

Non-radiative decay mechanisms introduce a high level of complexity in the analysis and predictability of fluorescence. Unlike radiative decay, of which there is only one type, numerous pathways of differing mechanisms exist for non-radiative decay, as illustrated in Figure 3 below. The practical considerations of this point are discussed further in Section 2.2. Timescales for critical fluorescence processes described in Figure 3 are further described in Table 1.

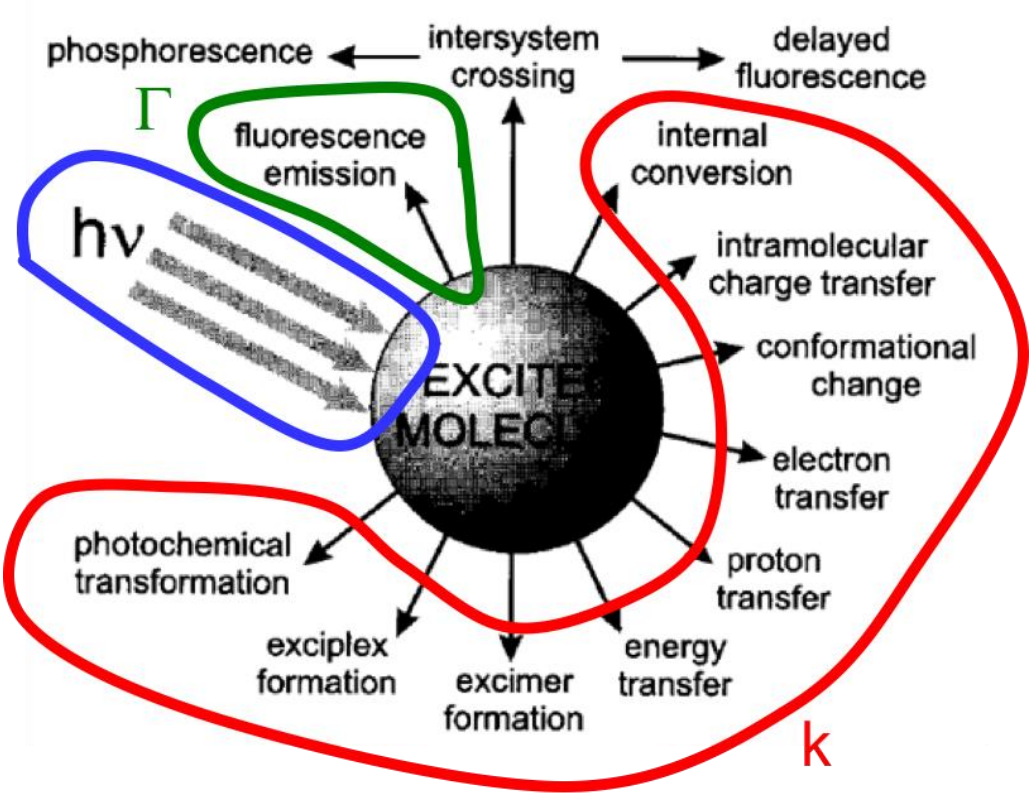

Figure 3 Summary of possible radiative and non-radiative decay mechanisms for the de-excitation of a molecule excited by electromagnetic radiation of energy hν, where Γ are radiative decay components and k are non-radiative decay components.

Internal conversion is non-radiative transition from a higher to a lower energy level, where electronic energy is converted into vibrational energy. Internal conversion generally increases with temperature, explaining the commonly detected decrease in fluorescence intensity with rising temperature. Molecular spin states are maintained during internal conversion, but change when transitioning between singlet and triplet states in a process called *intersystem crossing*. *External conversion* is where a fluorophore is deactivated non-radiatively and loses molecular energy through collisional interaction with its environment, for example colliding with other solute species.

Process	Transition	Timescale	
Light Absorption	S_0 to S_n	10^{-15}	*Femtoseconds*
Internal Conversion	S_n to S_1	10^{-14} to 10^{-11}	
Vibrational Relaxation	S_n to S_n	$10^{-12}$to 10^{-10}	*Picoseconds*
Intersystem Crossing	S_1 to T_1	10^{-11} to 10^{-6}	
Fluorescence	S_1 to S_0	10^{-9} to 10^{-6}	*Nano to microseconds*
Phosphorescence	T_1 to S_0	10^{-3} to 10^{-2}	*Milliseconds*
Non-Radiative Decay	S_1 to S_0 T_1 to S_0	$10^{-7}$to 10^{-5} 10^{-3} to 10^{-2}	

Table 1 Comparison of transition process timescales

2.1.3 Fluorescence Emission

Upon relaxing to the ground state S_0, a photon is emitted with energy $h\upsilon_{em}$. Where emission arising as a result of a molecule relaxing from a higher singlet state to the ground singlet state is termed fluorescence, emission arising from a molecule relaxing from a triplet state to the ground state is called phosphorescence[i]. As mentioned earlier, a molecule may exist in the triplet state after undergoing intersystem crossing.

Owing to energy dissipated through internal conversion, vibrational relaxation and external conversion, the energy of the emitted photon is lower than the $h\upsilon_{em}$ of the excitation

[i] Phosphorescence is a statistically more unlikely occurrence as the rate of intersystem crossing is low owing to the change of spin multiplicity required. Where it does occur, phosphorescence has both a longer lifetime (see Table 1) and a bigger Stokes shift, resulting from the lower energy of the triplet state.

photon. Photons are therefore emitted at a longer wavelength, in a phenomenon termed the Stokes shift. A Stokes shift allows emitted photons to be distinguished from excitation photons, and forms the basis for isolating background from excitation light to detect emission.

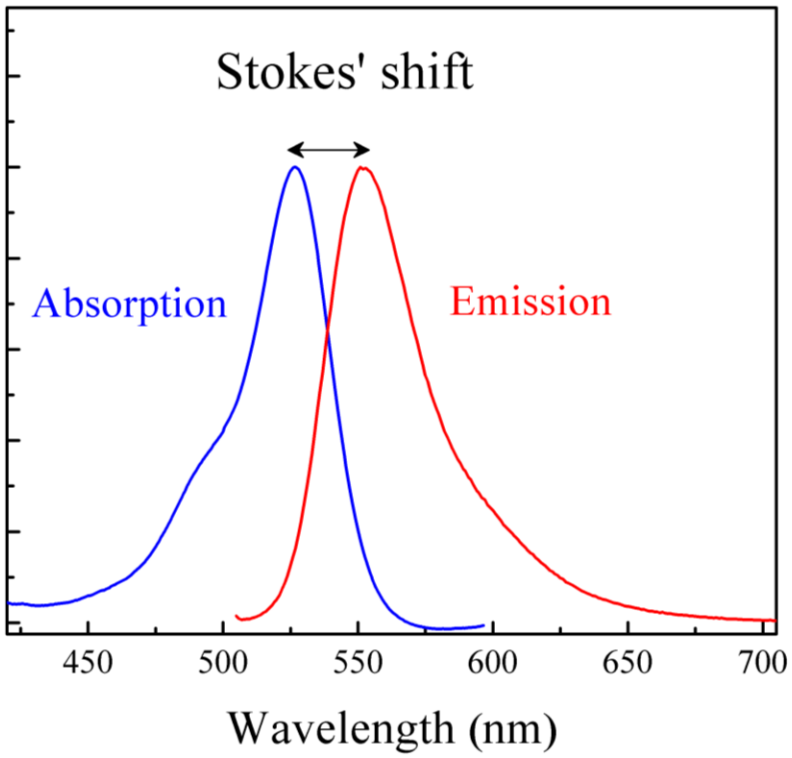

Figure 4 Absorption and emission spectra for Rhodamine 6G with a Stokes shift of around 25 nm. Stokes shift is the difference between the maxima of the absorption and emission spectra. (Source: Wikipedia)

2.2 Challenges of Describing Fluorescence

Any fluorescence observed may be described using four key concepts, although other parameters may also be used. Firstly, on a simple observational level, it can be described in terms of the (1) *wavelength emission*, or where on the spectrum it is emitting, and the (2) *intensity*, or how brightly the sample is emitting.

Another important parameter is the (3) *fluorescence lifetime*, τ. This is the time it takes for a molecule to relax from an excited state to the ground state, and is be defined by the total time taken for a combination of radiative and non-radiative processes to occur. τ may be denoted in numerical terms as roughly:

$$\tau = \frac{1}{\Gamma + k}$$

where Γ = radiative decay rates

k = non-radiative decay rates

Where decay processes are purely radiative, the intrinsic lifetime of the fluorophore, τ_0 can be defined as:

$$\tau_0 = \frac{1}{\Gamma}$$

A challenge of fluorescence, especially when it comes to quantifying information, is that not all components of the fluorescence descriptors above are intrinsic. Non-radiative decay processes are often dictated by local micro-environmental factors. For example, particular molecules such as oxygen are efficient at non-radiative quenching of fluorescence through external conversion. Similarly, changes in temperature and viscosity can impact on the amount of external conversion in a system. As such, when *k* must be described in terms of separate components;

$$k = k_{ic} + k_{ec} + k_{is}$$

where k_{ic} = rate of internal conversion

k_{ec} = rate of external conversion

k_{is} = rate of intersystem crossing

and an expression for k_{ec} may become further complicated simply by taking into account quenching alone;

$$k_{ec} = k_0[Q]$$

where [Q] is the concentration of the quencher, and k_0 is related to the diffusivity and hydrodynamics of reactants. This example serves to demonstrate how considering one component of non-radiative decay alone begins to complicate a descriptor such as fluorescence lifetime into a multifactorial entity beyond the realm of numerical predictability:

$$\tau = \frac{1}{\Gamma + k_{ic} + k_{is} + k_0[Q]}$$

Consequently, accuracy of quantitative analysis in fluorescence studies relies heavily on a fundamental understanding of the origin and mechanism of emission pathways[ii]. As

[ii] It is for this reason that in the biosciences, where fluorescence imaging already forms an important cornerstone of sample characterisation, strong emphasis is placed on the selection of an appropriate fluorescent dye. An intimate understanding of the emissive and absorptive properties of a dye benefits the experimentalist with an enhanced ability to interpret results, as well as the practical advantage of being able to optimise the data collection system being used, for example, by employing a more effective excitation wavelength or selecting a more apposite set of filters.

alluded to in Section 1, the project is therefore in part an exercise in assessing the suitability of advanced fluorescence imaging techniques to characterise catalytic samples where details of fluorescence properties are less widely understood.

A final important parameter is (4) *quantum yield*, which is a dimensionless ratio of the number of photons emitted per excitation photon absorbed:

$$\mathrm{Q} = \frac{number\ of\ photons\ emitted}{number\ of\ photons\ absorbed} = \frac{\Gamma}{\Gamma + k} = \frac{\tau}{\tau_0}$$

Quantum yield can be likened to a probability that a fluorophore will emit a photon, and will be a number ranging from zero to one, where unity represents a very bright fluorophore. While quantum yield is technically an intrinsic property when considered in the absence of a non-radiative decay component, in practice the parameter is similarly influenced by environmental factors like temperature, solvent properties, local pH and quenching rates.

2.3 Fluorescence Microscopy

Fluorescence microscopes are optical microscopes that use the properties of fluorescence (and sometimes phosphorescence) to generate an image.

2.3.1 Confocal

A confocal microscope uses the principles of fluorescence to detect light emitted from a sample. A basic microscope configuration is depicted in Figure 5a. A focused laser acts as the excitation source. It is directed onto the sample with a reflective dichroic mirror. The laser spot is rastered across the sample, such that an image is built up point-by-point.

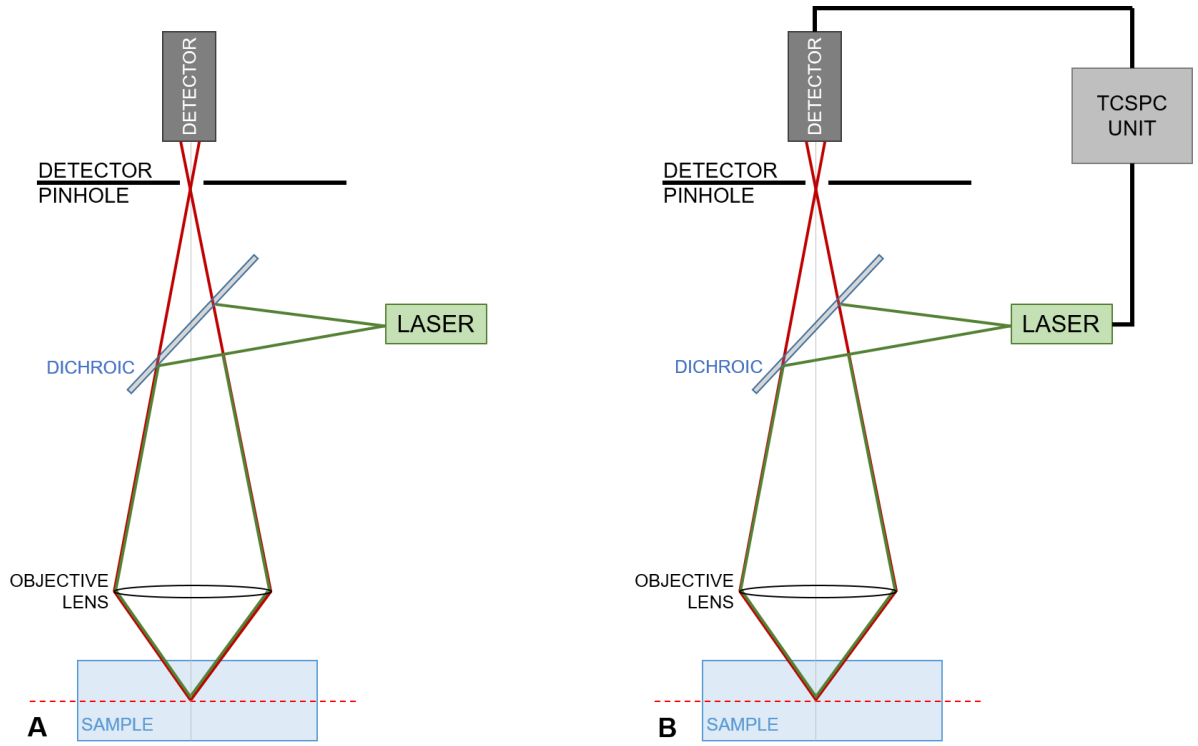

Figure 5 Schematic diagram of an A) Confocal Laser Scanning Microscope, and B) Fluorescence Lifetime Imaging Microscope

A confocal microscope is differentiated from a basic epifluorescence microscope through the use of a pinhole in front of the detector. The addition of a pinhole prevents out of plane light from convoluting the signal from the focal plane, as shown in Figure 6. A pinhole is not necessarily needed in front of the illumination source, as the lasers currently used in confocal microscopes can be sufficiently focused to a small enough spot size with the use of optics in an objective lens. However, as is the case for all optical microscopes, the excitation laser's spot size becomes a crucially important when considering factors such as resolution, optical sectioning thickness or photobleaching.

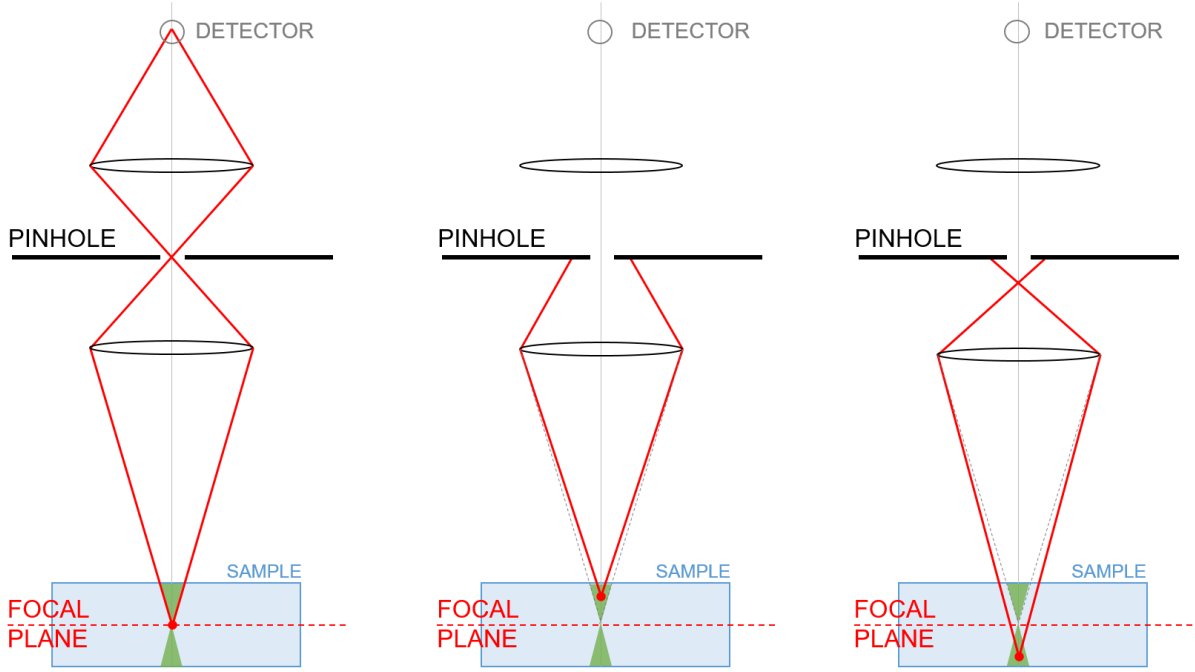

Figure 6 Schematic representation of elimination of out-of-plane light. With the addition of a pinhole, only light within a much smaller distance of the focal plane will be able to pass through to the detector. This is different to an epifluorescent microscope out of plane light is also liable to reach the detector convoluting the total signal received.

2.3.2 Fluorescence Lifetime Imaging Microscopy (FLIM)

FLIM is an imaging technique that maps fluorescence lifetimes pixel by pixel. As mentioned earlier in Section 2.2, the fluorescence lifetime is an important quantitative descriptor of the fluorescence emitted, and can be described as the amount of time the fluorophore spends in the excited state before returning to the ground state. It can be seen from Figure 5, the optical setup used is exactly the same as a confocal microscope, with the addition of a Time Correlated Single Photon Counting (TCSPC) card.

TCSPC[i] is a statistical technique that revolves around individually detecting a high volume of single photons, measuring their arrival times with respect to a reference signal and then reconstructing a histogram of photons detected with time. A statistically significant number of photons must be collected for this technique to work. In a simpler analogy, TCSPC could be likened to a stopwatch, where a starting pulse signals the beginning of the measurement, after which point the detection system starts recording the arrival of photons, and a stop pulse signals the end of the measurement. Table 1 of Section 2.1.2 allows us to better appreciate the brevity of timescales on which fluorescence occurs, and the exactitude required to make such measurements as detecting the arrival of a single photon. For this reason, a FLIM system always employs a pulsed laser, which both excites the sample and provides the timing signal required to generate a FLIM measurement. A pulsed laser has the added benefit of being

able to run at a higher average power than a continuous wave (CW) laser, as the sample is only being intermittently bombarded with excitation energy. It should be noted that in the case of a standard confocal microscope, either a pulsed or continuous wave (CW) laser may be used.

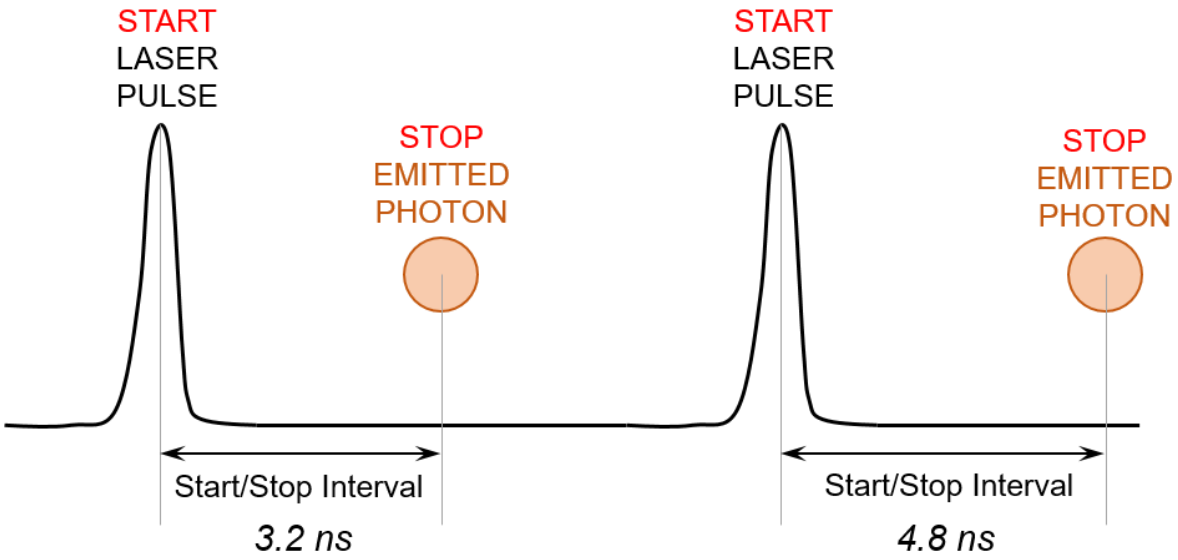

Figure 7 Schematic diagram with a laser pulse representing the start pulse and an emitted photon representing the stop pulse. The (here arbitrarily numbered as 3.2 and 4.8) start/stop intervals will be collated and reconstructed into a histogram.

2.3.2.1 Principles of TCSPC Electronics

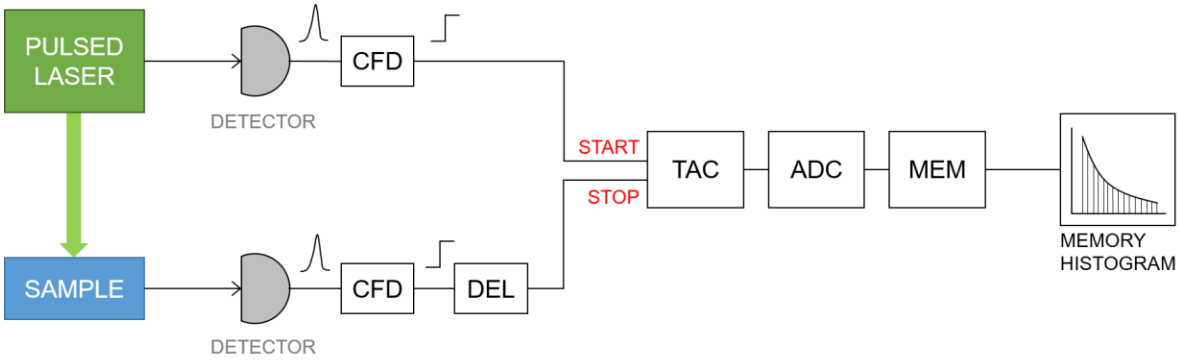

Figure 8 Major electronic components in TCSPC signal processing

As shown in Figure 8, the main electrical components on a TCSPC card for signal processing are a Constant Fraction Discriminator (CFD), electrical delays (DEL), Time-to-Amplitude Converter (TAC), Analogue to Digital Converter (ADC), and digital memory (MEM).

The system receives two inputs; the start signal direct from the laser and the input signal emitted from the sample. At first, the electronics evaluate pulse height and discard pulses below a given threshold to eliminate small amplitude noise. The CFD then analyses and normalises the pulse shape of individual pulses, to extract timing information from pulses of variable amplitude. This information allows the system Instrument Response Function (IRF) to be more

finely tuned. The CFD analysis is especially important when the detector is a photomultiplier tube (PMT), as the pulse amplitudes can vary significantly.

Normalised pulses from the CFD are then fed through to the TAC, which is a linear ramp generator initiated and halted by the start and stop signals respectively. The resulting output is voltage proportional to the time difference between the two signals. Voltage from the TAC is fed to the ADC, which assigns digital timing values to allow the reconstruction of the histogram. All measured TAC pulse amplitudes are sorted into different time bins. The ADC resolution will determine how many discrete time values are allowed, although higher resolution generally means that processing power must be exceedingly fast to prevent lag in the system.

3 Literature Review

3.1 Zeolites

Zeolites are aluminosilicate mineral frameworks formed by condensation polymerisation under hydrothermal conditions. Their crystalline microstructure is characteristically porous, with internal channel and/or cage-like structures ranging in diameter from around 0.3 to 1.5 nm [1]. Zeolite porosity is an important factor in their catalytic activity, as the channels are capable of hosting a variety of cations, and small molecules. Approximately 230 unique structural permutations of different zeolite frameworks are known to exist, the bulk of which are formed industrially rather than naturally. The Nickel-Strunz classification can be used to sort zeolites into different structural groups, a selection of which are pictured in Figure 9.

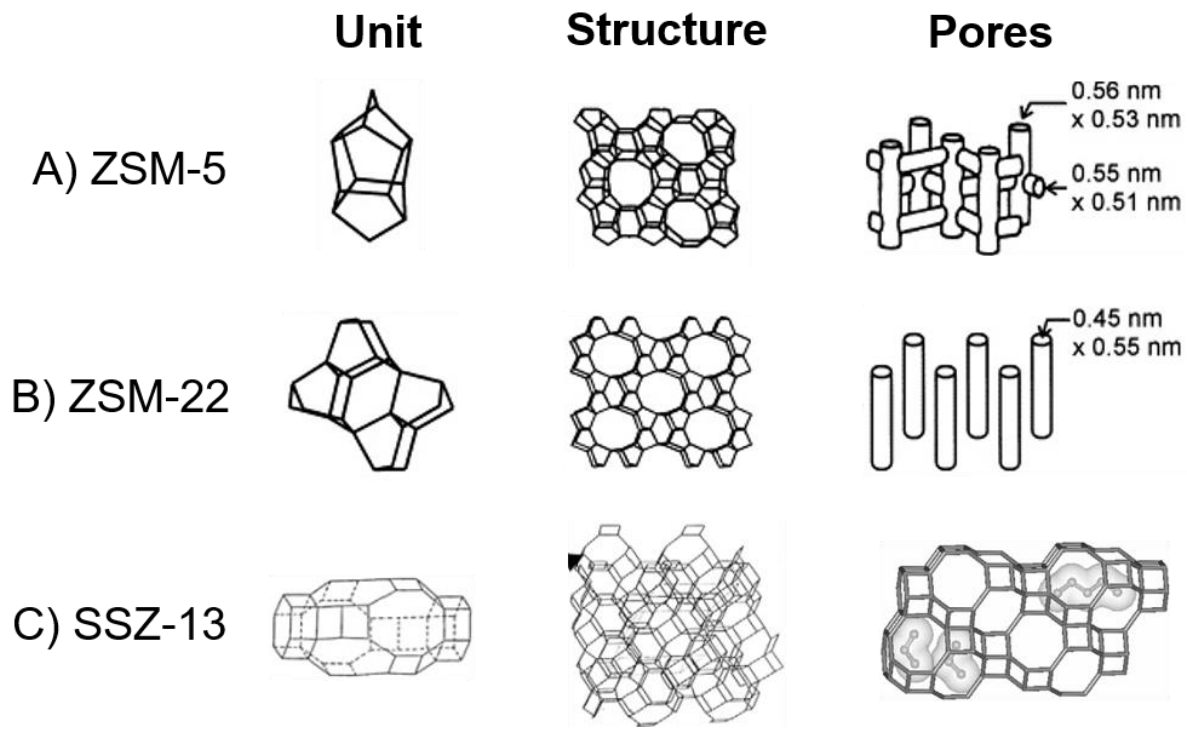

Figure 9 Examples of three zeolite topologies A) ZSM-5; pentasil unit structure which gives rise to a network of medium sized pores, B) ZSM-22; features unidirectional pores, C) SSZ-13; featuring a more cage-like pore structure capable of trapping smaller molecules

ZSM-5, which features in several of the literature examples below and form the basis of primary studies included in Section 4, is a synthetic zeolite consisting of pentasil units linked by oxygen bridges. Of structural importance to ZSM-5 are the 5.4-5.6Å diameter medium sized pore channels, which provide good size selectivity in isomerization reactions. Its use in the petrochemical industry as a catalyst for methane conversion reactions mean that it is commonly

researched as a model system in literature. By contrast, SSZ-13 has a more cage-like structure that can be better suited to trapping bulkier molecules, demonstrating the range of shapes zeolites can be synthesised in.

Zeolites are widely used in the petrochemical industry in the conversion of methane to hydrocarbon reactions (MTH), where methane is catalytically oxidized to light olefins such as ethane and ethylene, or the related methanol to olefin (MTO) reaction. In the majority of these reactions, catalysts become deactivated over time with the build-up of coke deposits. Although oxidative catalyst regeneration may be employed to reverse the coke deposition process, repeated regeneration eventually leads to a degeneration of the zeolite crystallinity that in turn renders the catalyst lifetime finite[2].

Both the compositional nature and deposition process of the coke are complex and yet to be experimentally verified. This difficulty relates to the lack of imaging modalities that can successfully resolve carbonaceous materials on a relevantly small nanometre length scale required for catalysis. Where a non-reacted sample is white, a reacted sample appears pitch black. Traditional electron imaging modalities, for example, do not resolve this visual discrepancy.

3.2 Fluorescence Microscopy in Catalysis

Imaging catalysts with fluorescent microscopy is a method that has gained momentum in the last decade, following pioneering work by Calzaferri *et al* (see Section 3.2.1). Approaches are both novel and diverse, with results ranging from the visualisation of single catalytic events to the beginnings of super-resolution [3]. Results obtained in the field so far are not, however, without their limitations. The extensive use of esterification to image catalytic events exclusively on Brønsted acid sites (see Section 3.2.2.1) and the use of highly engineered samples (see Section 3.2.2.2) highlight the challenges facing the field in finding more flexible imaging modalities that can be used for industrially relevant catalysis samples.

3.2.1 Pioneering Studies

Two pioneering studies have been selected here to highlight the early development of fluorescence techniques. First, an early pioneering study by Calzaferri *et al.* in 2003 showed that fluorescent dye molecules could be successfully aligned along the narrow pores of zeolite L, and moreover be imaged successfully with basic spectroscopic equipment[4].

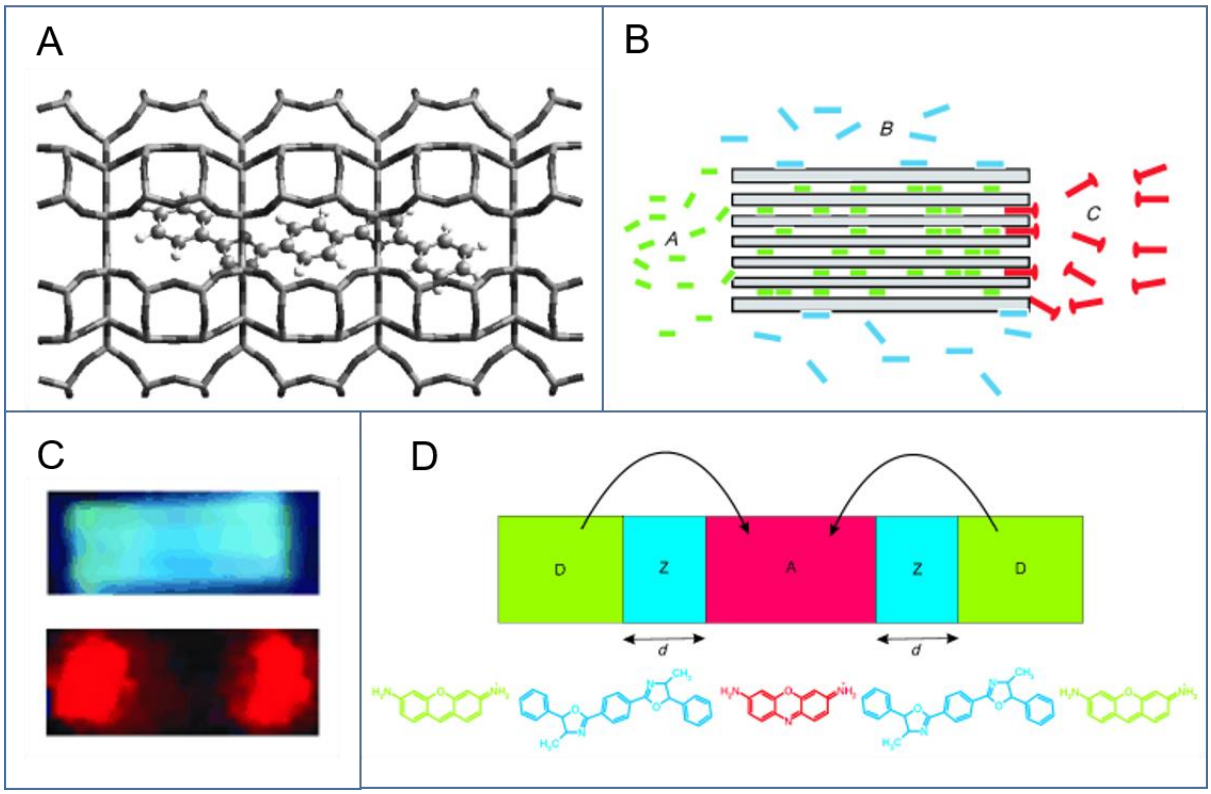

Figure 10 A) Schematic demonstrating the alignment of POPOP dye molecules in the channels of zeolite L. B) Diagram demonstrating three ways of loading dye into the pores of zeolite L, with green representing dye molecules that have reached equilibrium by insertion, blue for molecules that have adsorbed and red for molecules that adsorb specifically like a stopcock at a channel entrance. C) Fluorescence images showing top: DMPOP dyes inserted into zeolite L in blue and bottom: Ox+ dyes plugging the channel ends in red. D) The ultimate application of dye loading as antennae.

This was an important publication, as it showed that the fundamental structure of the zeolites could be positively harnessed, and moreover begin to provide structural specificity in the images obtained. Further being able to relate the alignment of transition dipole moment to determine the polarisation of fluorescence, the research demonstrated the manifold ways in which internal structure and crystallographic orientation could be observed using this method. A further review by Calzaferri on the same topic showcases how dyes were loaded, but how zeolite antennae loaded with dyes could be coupled to polymers to create a device of macroscopic proportion[5].

A second early study was conducted by Roeffaers *et al.* the location of catalytic sites was directly imaged by converting fluorescein esters to fluorescein at basic sites in layered double hydroxide (LDH) crystals using widefield fluorescence microscopy[6]. The real-time *in situ* conditions under which data was obtained made this experiment one of the first fluorescence experiments directly addressing the observation challenges of heterogeneous catalysis. By comparing the tendency for absorption and desorption to occur on different crystallographic

planes of the LDH crystals, it was concluded that catalysis was occurring at defect sites. The methodology used here also had clear advantages over Transmission Electron Microscopy (TEM) and Scanning Tunnelling Microscopy (STM), as it was able to operate at ambient temperature and pressure in a condensed phase without the need for a conductive surface.

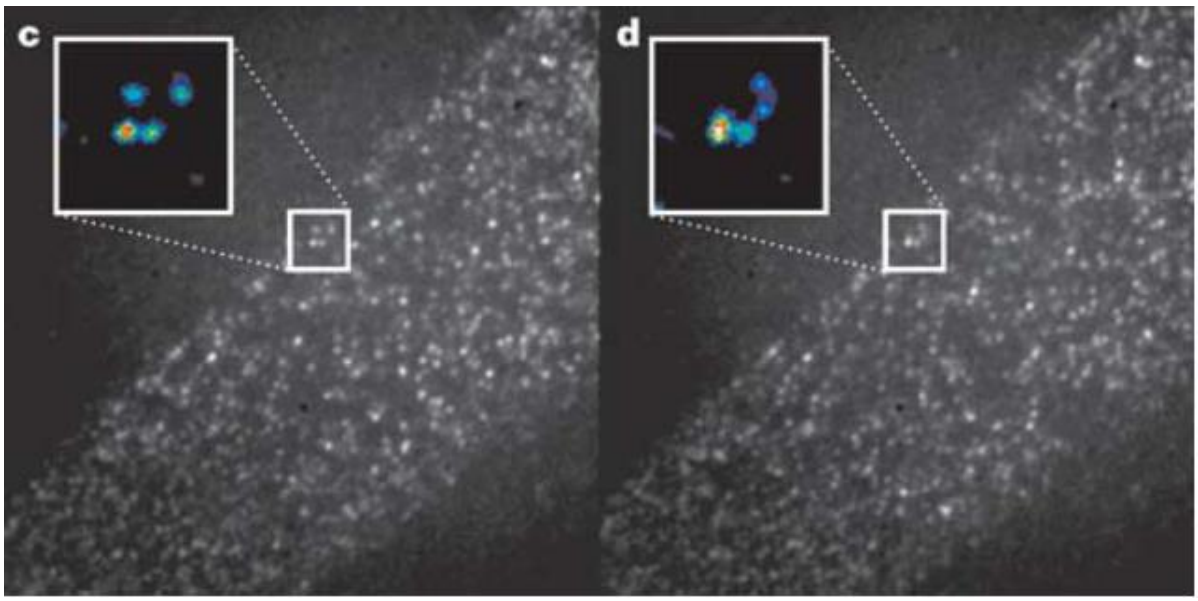

Figure 11 Wide field *in-situ* fluorescence images of C-FDA transesterification on propyl amine-functionalised cover glasses. Bright spots highlighted correlated with newly formed products, with image d being taken 100 ms after image c.

3.2.2 Imaging in Zeolites

3.2.2.1 Using an Introduced Dye

Building on the research mentioned in Section 3.2.1, In the case of inorganic heterogeneous catalysts, a single particle will likely have a high number of individual catalytic centres distributed across both external and internal surfaces, each of which will have varying degrees of accessibility[iii] and types of chemical properties. A significant body of work by Weckhuysen *et al.* utilises furfuryl alcohol oligomerisation onto Brønsted acid sites to create fluorescent products, typically in ZSM-5 crystals, which are subsequently imaged using a selection of methods. This tagging method has been used variably to highlight features of catalyst structure, as well as to create super-resolution images, that is images that bypass the approximate 250 nm diffraction limit of a traditional optical microscope.

[iii] Consider the porous cage-like molecular sieve structures of a zeolite or metal-organic framework; certain channels will be accessible to some molecules and not others depending on the size.

Furfuryl self-reaction was used in a mordenite crystal to image reactive zones at different crystallographic angles[7]. This early study was used to flag the potential of fluorescence microscopy as an *in situ* characterisation technique in catalysis.

In their super-resolution studies of ZSM-22, Roeffaers et al. are able to resolve needles with a thickness of less than 100 nm [8]. In this work they also introduce their technique of Nanometre Accuracy by Stochastic Catalytic Reactions Microscopy (NASCA), which appears in a number of their later papers. Bearing subtle similarities to super-resolution techniques such as Stochastic Optical Reconstruction Microscopy (STORM), NASCA involves recording a series of individual catalytic events and later using mathematical fitting to reconstruct a reaction map from individual reaction sites with respect to x and y positions. The NASCA technique was further utilised in the real-life catalysis scenario of fluid catalytic cracking. In this instance, zeolite Y and ZSM-5 were again tagged with furfuryl acid and excited at 532 nm to create a sensitive cluster analysis of zeolite structures [9].

Aramburo *et al.* used larger non-reactive dyes and staining reactions to study the effect of steaming on acidity in large ZSM-5 zeolites [10]. Using this method, it was possible to image cracks and defect mesopores arising in steamed zeolite crystals.

3.2.2.2 Utilising Autofluorescence

Fluorescence imaging in zeolites has also been carried out where fluorescence already occurring in the sample, or autofluorescence, is utilised for imaging, rather than in earlier works where either dyes or esterification reactions were used to create fluorescent events. The origin of the sample's natural fluorescence is variable. An early study by Karwacki *et al.* utilised fluorescence speculatively associated with alkyl amine templating to observe changes in fluorescence during de-templation [11].

As mentioned in Section 3.1, a major problem facing zeolites in industry is the phenomenon of coking, which both deactivates the catalyst and renders its ultimate lifetime finite. Coke deposits formed in the methanol to olefin (MTO) reaction are fluorescent, likely due to their aromatic ring structure[12]. Two similar studies of utilising similar techniques piloted by Karwacki *et al.* to image coke deposition in large H-ZSM-5 crystals were conducted by Chung *et al.* and Nordvang *et al.* In an earlier precursor study, the formation of coke deposits during the aromatisation of C4-C7 paraffin was visualised over micron-sized H-ZSM-5 crystals [13]. In this study it was concluded that paraffinic reactants converted mainly along crystal boundaries, while olefinic hydrocarbons built up inside the crystal. A later study by Nordvang

focused on coke deposition arising as a result of the MTO reaction [14]. Changes in fluorescence could be related to deactivation of the catalyst and it was postulated that formation of poly-aromatic species on the external surface were the reason for this deactivation.

In both instances, the techniques utilised highlighted a strong spatial variations in fluorescence intensity across the samples, and enabled the groups to visually identify regions of the samples where catalytic activity seemed more abundant (most notably at the edges of the crystal, and through the centre of the crystal, where heightened intensity was observable along internal crystal boundaries). Data from the Nordvang study in Figure 12B took full advantage of a confocal microscope's ability to z-section a sample, to highlight regions of the crystal where fluorescence activity was highest. Both the catalytic model systems selected and the use of a temperature controlled reaction cell on an optical microscope stage also act as important precursors to the work that has been carried out in the current project so far (see Section 5).

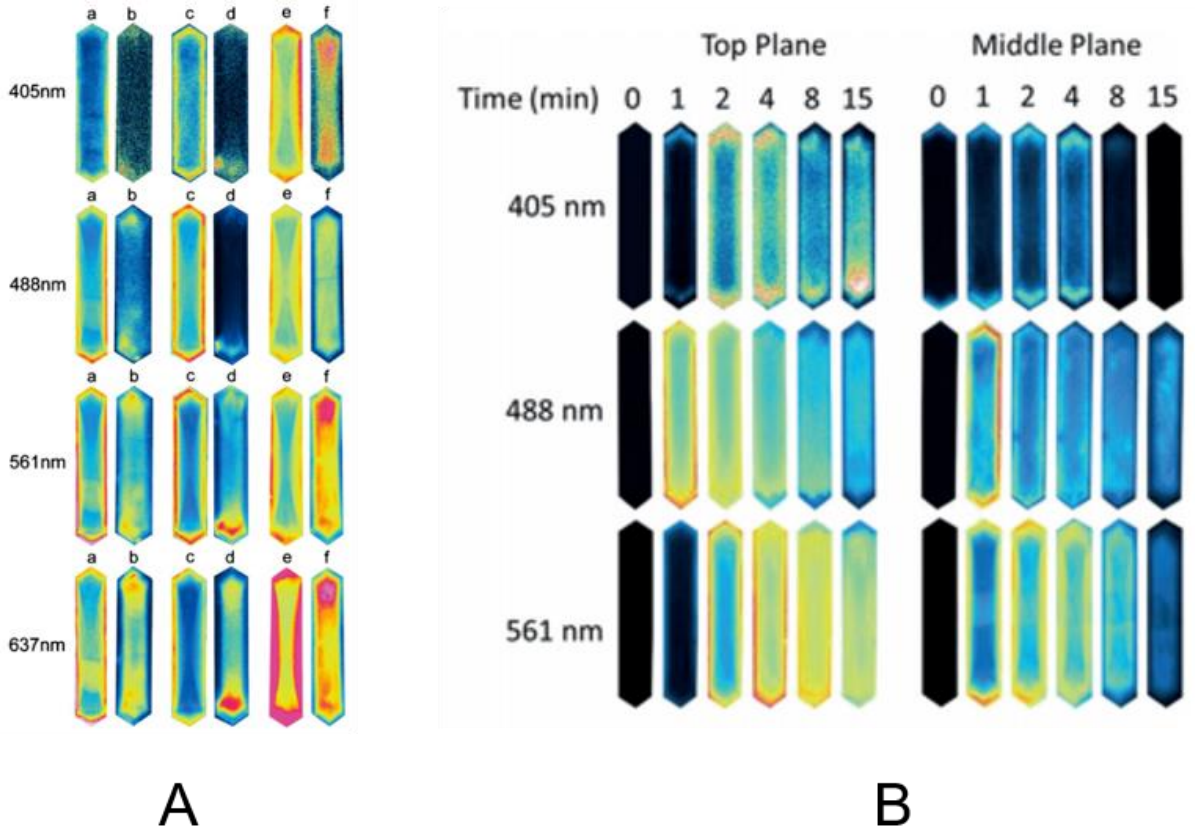

Figure 12 Series of confocal images where colour correlates with intensity in the A) Chung study where fluorescence images of H-ZSM-5 during the aromatisation process at 773 K for a) pentane, b) pentene, c) 2-methylpentane and d) 2-methyl-2-pentene, and B) Nordvang study where crystals were excited with 405, 488 and 561 nm excitation at different time points in the MTO reaction. Adapted from [13][14]

3.2.3 Imaging in Reactors

In the realm of photocatalysis, fluorescence imaging was utilised by Wang et al. as a mass screening device to evaluate the catalytic performance of a material deposited on a micro-reactor chip. A change in fluorescence intensity with time could be correlated with areas on the substrate of higher catalytic activity [15]. The images obtained were of a lower resolution and not focused on finding information about catalytic structure, but rather to assess in a more industrial manner the performance of photo-catalysts being produced. This study represents a more practical application for fluorescence imaging in catalysis.

3.3 Conclusion

Although a body of prior literature can be found, it remains that the use of fluorescence microscopy in catalysis is a relatively under-researched area. A first point to note is the vast number of advanced fluorescence and super-resolution microscopy techniques that have not yet been attempted on catalytic systems such as Fluorescence Lifetime Imaging (FLIM), STORM, Stimulated Emission Depletion microscopy (STED) or Structured Illumination Microscopy (SIM). This project so far attempts to address this issue by trying samples in each of the mentioned techniques.

Secondly, fluorescence images obtained tend to be qualitatively rather than quantitatively imaged. As the majority of the studies revolve around exploring structure, the valuable information obtained relates, on a chemical level to the appropriateness of the dye selected, and on a microscopic level to the degree of resolution enhancement achieved through different effects. With the combined use of methods such as FLIM, spectral detection, and the potential to correlate images with different microscopes, this project should yield more relevant images capable of being quantitatively with respect to intensity and fluorescence lifetimes.

Thirdly, most of the prior research completed has been performed on static samples that have been removed from their reaction conditions. Especially in the case of ZSM-5 studies, previous research has utilised large crystals up to 100 μm in size. Work to date on this project bears strong similarity to that shown in Section 3.2.2.2, especially with respect to experimental setup. Marked improvements to this experiment however include the use of industrially relevant powdered ZSM-5 rather than intergrown crystals, the use of a more advanced FLIM techniques which yields both a confocal image and a map of fluorescent lifetimes, and the development of a tailored reaction cell to give more catalytically relevant information.

4 Preliminary Characterisation

As catalytic samples are not frequently characterised using optical microscopy techniques, a range of preliminary testing was carried out to determine what imaging methods would be best suited to extracting novel, meaningful information from catalytic materials. Testing was carried out on 4% Mo/H-ZSM-5 samples, and H-SSZ-13 samples, each coked to varying degrees. 4% Mo/H-ZSM-5 samples were created by loading zeolite framework with molybdenum by manually grinding a powder ZSM-5 with an Si/Al ratio of 30 (CBV 3024E, Zeolyst International) with powder MoO_3 for 30 minutes to induce a solid state exchange reaction. The catalysts are calcined at 700°C for 30 minutes prior to starting any reactions under methane gas. Batches of the sample were reacted under CH_4 gas at 700°C for 4, 9, 25 and 75 minutes.

4.1 Emission Spectra

Information on the emission and excitation spectra is important for imaging, as it indicates what the optimal excitation wavelength for a laser might be, and informs how filters in the microscope should be configured to specify detection windows. In the first instance, obtaining an excitation and emission spectra was attempted in an Agilent Cary Spectrophotometer. Despite prepping the solid sample in a front-facing configuration, as shown in Figure 13B, and preparing a solid suspension in liquid to be tested as in Figure 13A, satisfactory signal could not be obtained. This could be related to a high degree of scattering off the solid particle, or perhaps the power of the excitation light was not sufficient.

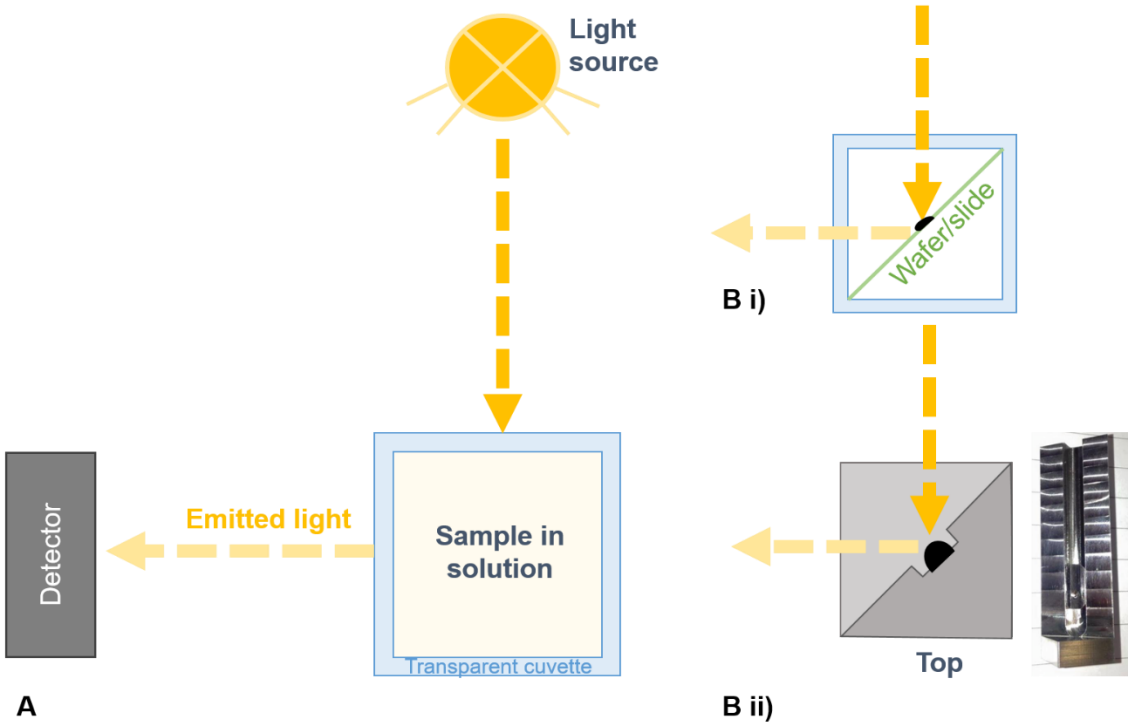

Figure 13 A) A basic diagram of a spectrophotometer configuration. A light source illuminates an optically transparent cuvette that is typically filled with a solution of the sample. A detector is positioned at 90 º to the light source to ensure only light emitted from the sample is detected and reduce direct signal from the light source. B) Shows two front-facing configurations for solid samples with i) demonstrating an option where solid sample was mounted on a glass slide and positioned 45º to the light source and ii) A metallic cuvette with an enclave for a small amount of sample to sit.

An emission spectrum for the sample was instead obtained on a Kerr-gate Raman system. Kerr-gating is a technology that uses temporal gating to filter out fluorescent signal and gain access to weaker signals such as Raman. The custom built in-house set up[16] was used to obtain emission and Raman data. A 10 kHz 400 nm excitation laser with a 100-150 µm spot size and laser power of 100 mW near the sample surface. A 300 µm slit with 150 l/mm grating and 500 nm blaze was used. In the case of the emission spectrum, gating times ranging from -10 to 500 ps were used, and selected traces were included in Figure 14.

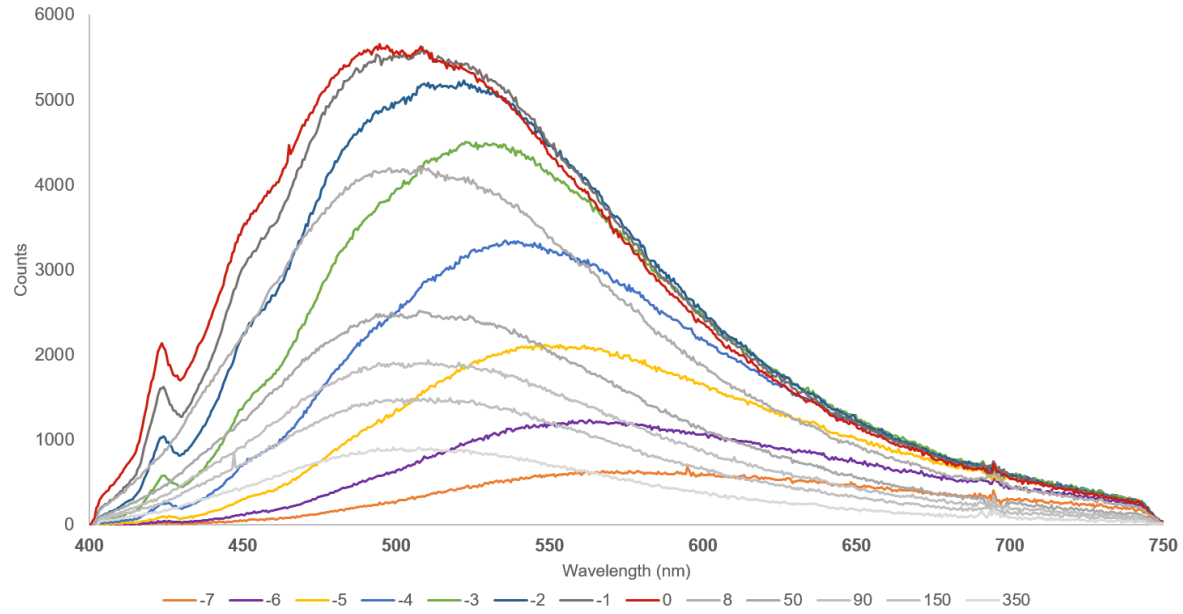

Figure 14 Kerr-gate Emission Data of 75-minute 4%Mo/H-ZSM-5 at 400 nm

The samples tested here are Mo doped H-ZSM-5 framework that has a high degree of coking owing to a relatively long reaction time of 75 minutes. Figure 14 shows that the samples are broadly emitting, with a peak spanning from around 480 to 530 nm. The origin of the fluorescence could be attributed to either the zeolite framework, the carbonaceous species, or a combination of the two.

4.2 Electron Microscopy

4.2.1 Scanning Electron Microscopy (SEM)

SEM was carried out on 4% Mo/H-ZSM-5 samples. This method was selected for its high resolution and ability to image surface morphology and shape.

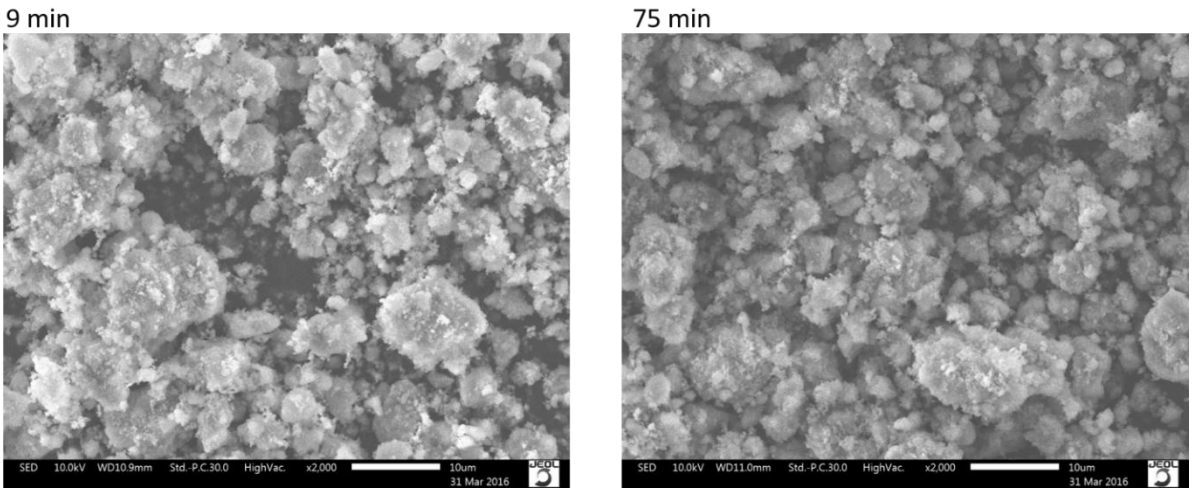

Figure 15 JEOL JSM-IT300 SEM images of A) 9-minute reacted 4%Mo-H-ZSM-5 and B) 75-minuted reacted 4%Mo/H-ZSM-5

SEM shows that crystals range in size from around 10 µm in diameter to sizes less than the resolvable diffraction limit of 200 nm. Crystal shapes are irregular, and there is an observed tendency for crystals to agglomerate. Although to the naked eye there is visibly more coking on the 75-minute sample compared to the 9-minute sample, in SEM the samples look almost indistinguishable.

4.3 Fluorescence Microscopy

4.3.1 Confocal

Figure 6 shows confocal microscopy at different visible excitation and emission wavelengths. These images were taken on a customized inverted Nikon TE2000U microscope with a Nikon EC2 confocal scan head. Different excitation sources were used, as specified in the figures. For FLIM, images were acquired at 256x256 pixels.

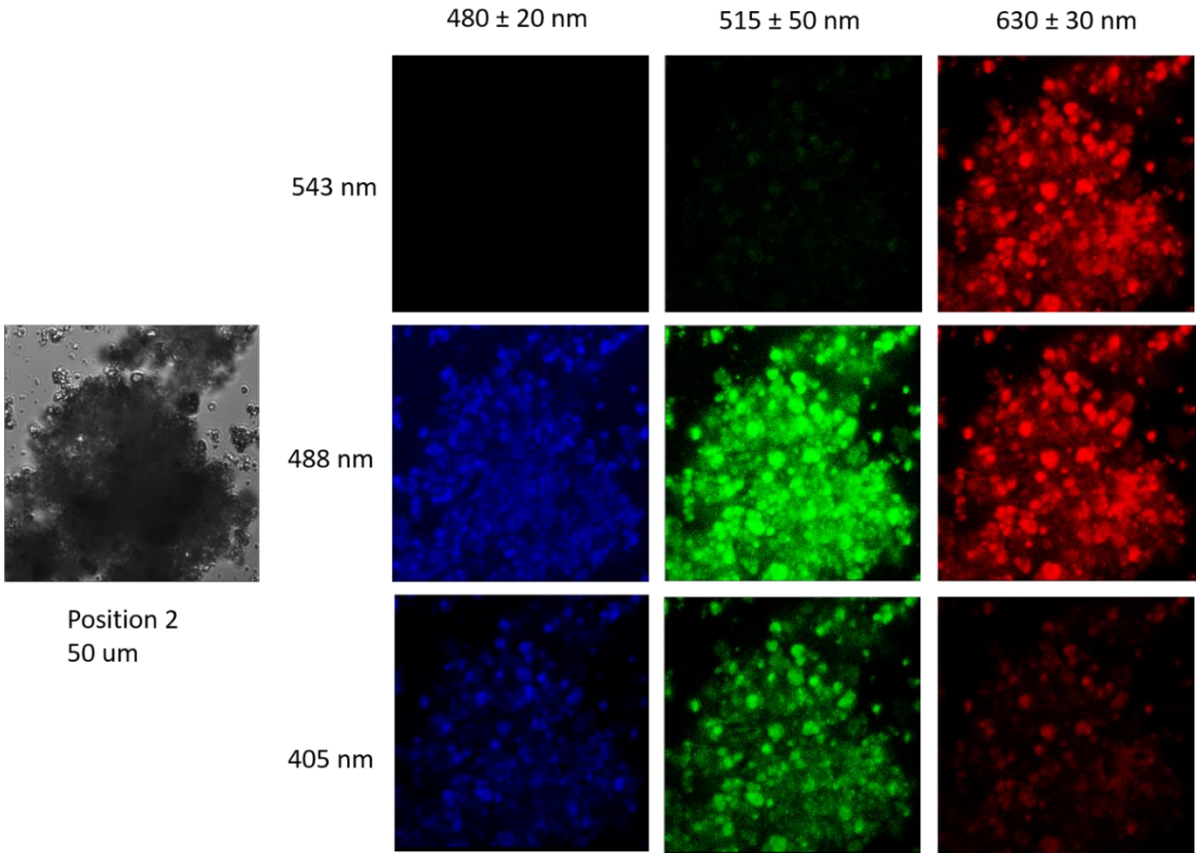

Figure 16 RGB channel confocal microscopy image of 75-minute reacted 4%Mo/H-ZSM-5. In the white light transmission image the black powder can be seen. Confocal imaging shows a range of structures not visible in transmission. Emission becomes red-shifted as excitation wavelength increases, with almost no blue or green emission at 543 nm.

A comparison of SEM and a confocal (lowest pinhole setting, 30 µm, 0.25 airy units) is shown in Figure 8. Images on a similar length scale show how the small bright areas in confocal may correlate with the structures observed in SEM.

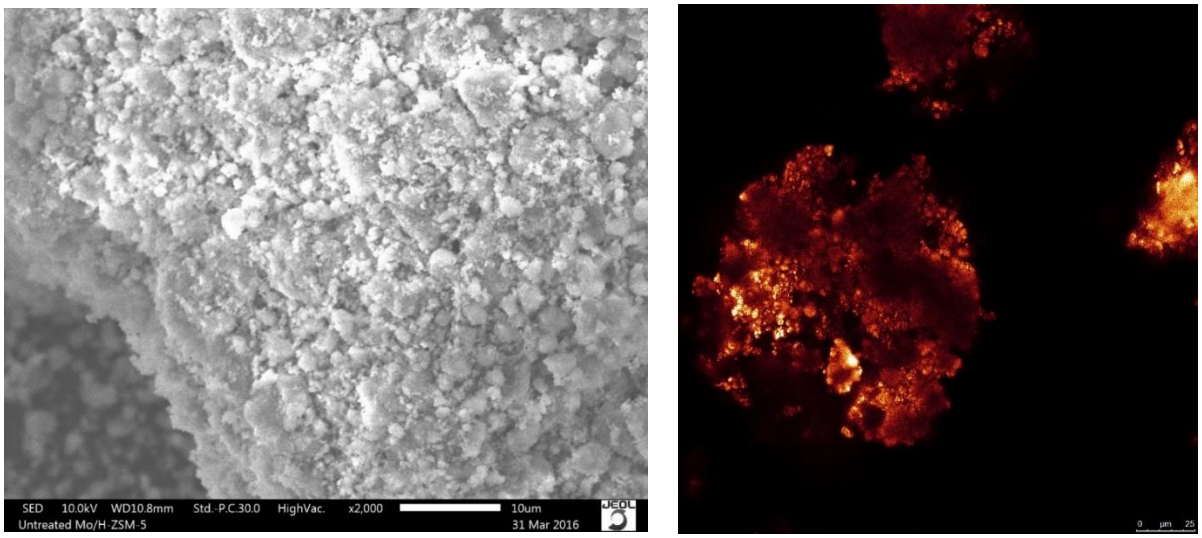

Figure 17 A) x2000 SEM image of 75-min 4%Mo/H-ZSM-5 showing a larger aggregate of powder B)Confocal image of 75-minute 4%Mo/H-ZSM-5

4.3.2 Fluorescence Lifetime Imaging (FLIM)

Preliminary FLIM imaging shows that from the fluorescence observed in confocal, a number of different lifetimes exist. Lifetimes observed in this image range from 750 ps to longer lifetimes of over e2000 ps. Additional data indicates shorter lifetimes than 750 ps may exist. FLIM was also successfully characterized with 737 nm multiphoton excitation, indicating that excitation at around 370 nm may be occurring.

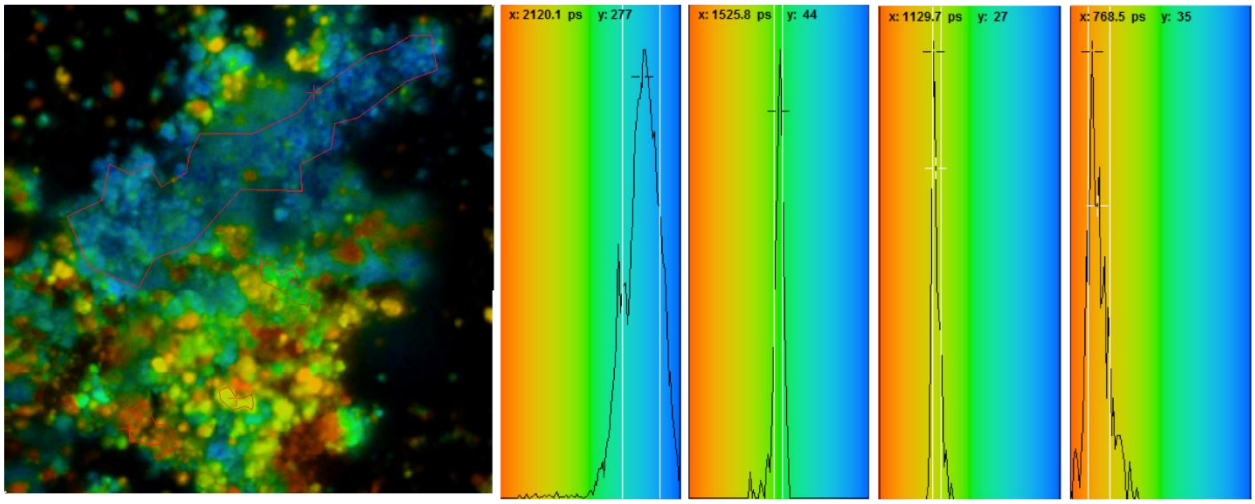

Figure 18 Single photon 405 nm excitation FLIM image of 75-minute 4%Mo/H-ZSM-5 sample showing lifetimes ranging from around 750-2000 ps

4.3.3 Super-resolution Microscopy

Super-resolution is a class of fluorescence microscopes that are able to surpass the diffraction limit of a standard optical microscope. Achieving super-resolution of catalytic

material is of particular interest as probing a nanostructure may give better information on how crystallographic form relates to catalytic function.

STED was not able to successfully image the coked 4%Mo/H-ZSM-5. The major challenge for imaging catalysts using the STED technique is the high power density of the depletion beam (~300mW in a 250nm focus spot size). The autofluorescent aluminosilicate zeolite crystals used are black in appearance, meaning they will absorb the high power depletion beam. In effect, this results in the sample rapidly heating up and blistering on the coverslip within a few seconds. This effect is observed even on the lowest laser power setting of 0.1%. Beyond this, the broad autofluorescence of the samples also poses a challenge for STED imaging, where the highest resolution is obtained with increasing depletion laser power.

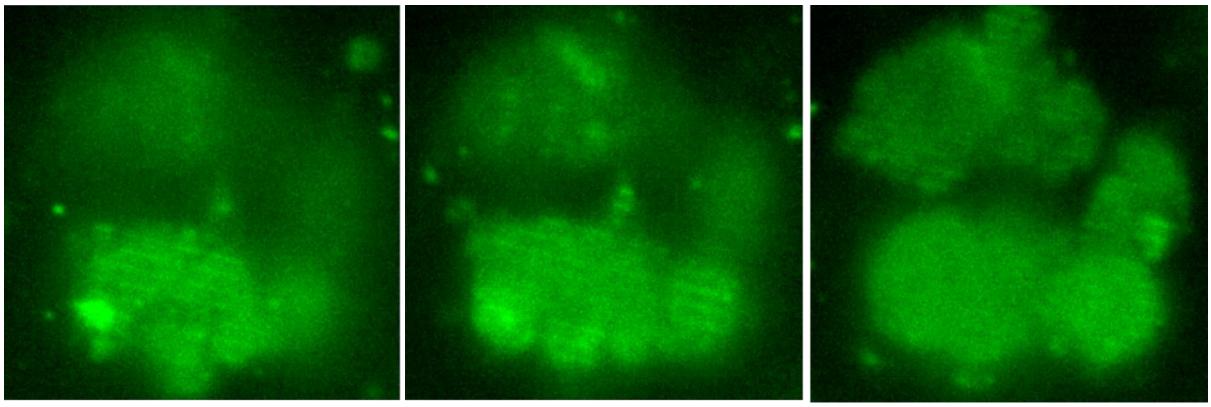

Figure 19 SIM images of 75-minute 4%Mo/H-ZSM-5 with 16.5 µm field of view; Apoochromat 63x/1.4 oil objective, □$_{ex}$□□□561nm, pixel time =1.6 s, frame time = 4.06 s

Figure 20 shows images obtained from a novel super-resolution add-on module designed to be fitted to a Nikon confocal scan head from a company named Bioaxial. Similar in effect to Zeiss' Airyscan[iv], Bioaxial's CODIM-100 module claimed to improve resolution on confocal images to around 130 nm.

[iv] Samples were imaged in Airyscan, but no significant improvement was observed over the confocal image.

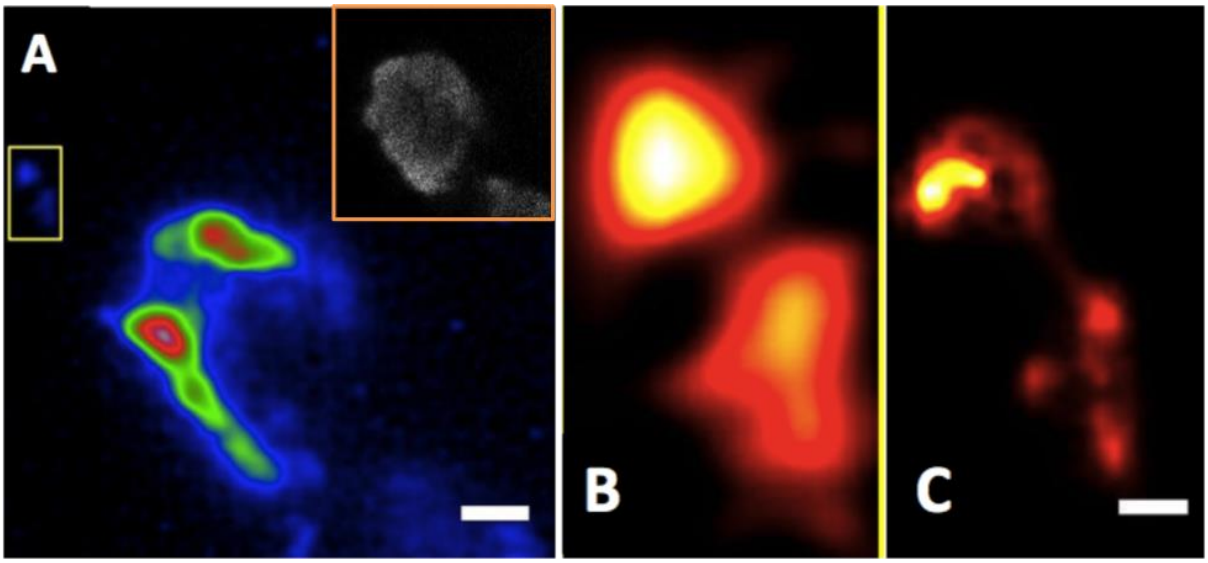

Figure 20 A) Grey image in top right shows the original confocal image; blue region uses the maximum-a-posteori (MAP) deconvolution algorithm where the green/red utilize the least square estimate (LSE) deconvolution based on the Monte-Carlo law. The image is a 10 x 10 µm area with a 1 µm scale bar. B) Cropped area of the MAP deconvolution and C) Same area using LSE reconstruction with 500 nm scale bar.

Although the Bioaxial system showed some improvements compared to the confocal system, at around 150 nm, the resolution is below that required for catalysis studies. As the system is highly dependent on post-processing to enhance the images, there is the possibility that improved algorithms in the future will be able to provide better iterations of the original data sets. As shown in Figure 10, work on a new deconvolution method resulted in a better quality image. In the future with more development, this method may yield more promising results, although processing would need to be able to resolve images down to at least 50 nm to be of serious interest.

4.4 Conclusion

Of all the imaging modalities trialled, FLIM generated a promising set of images. Although the potential structural information that could be gained from nanometre resolved super-resolution images remains of indelible interest, the inhomogeneity of contrast captured across coked 4%Mo/H-ZSM-5 samples was compelling enough for a successful beamtime application to be submitted. There is intention to pursue super-resolution experimentation further at a later date, as a complement to information that has and will be collected from recent and future FLIM beamtime experiments.

5 In-situ FLIM imaging of MTO reaction

5.1 Aim

The aim of this experiment was to observe *in situ*, in what would represent an experimental first, a change in fluorescent lifetimes H-SSZ-13 catalysts undergoing the methanol to olefin reaction.

5.2 Experimental Setup

5.2.1 Microscope Configuration

A modified[v] FTIR600 Linkam cell with CaF_2 windows was mounted onto a Nikon TE2000U microscope stage. A High-Resolution Optem x20 (NA 0.6, WD 13 mm) was used to accommodate the longer working distance. A Becker & Hickl HPM-100-40 high speed hybrid detector for TCSPC was interfaced with the Becker & Hickl SPC-150 TCSPC card to form the detection side of the microscope. An 80 MHz 405 nm pulsed single photon laser source was used to excite the sample.

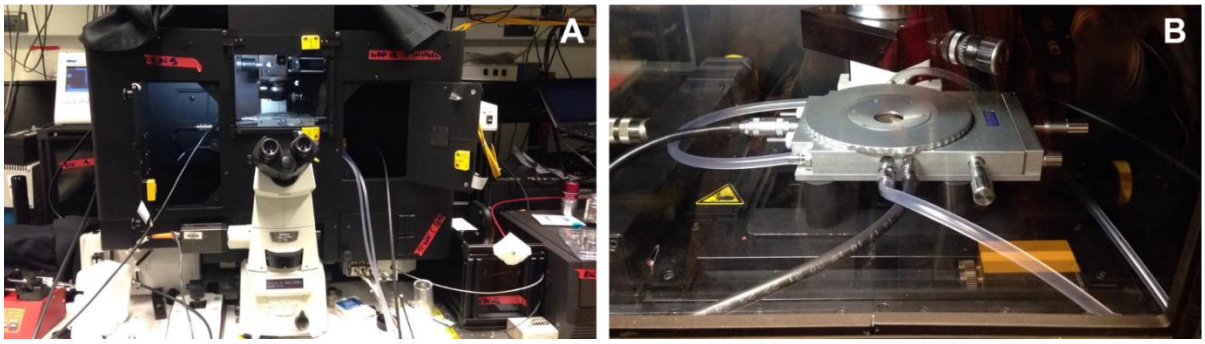

Figure 21 A) Front view of Nikon TE2000U with a black laser safety enclosure built around it and gas lines fed through the doors. B) A close up of the Linkam cell connected to tubing. Clear tubes carried water through the cooling channels, the black cable on the left connects to the temperature controller, and the black tubes on the anterior and posterior aspects of the cell form part of the gas lines.

5.2.2 Gas Line Configuration

Two gas bottles were used; one of 20% O2 in He to activate the catalyst, and one of He to purge lines and act as a carrier gas for vaporised methanol. Gas lines were configured as shown in Figure 22.

[v] This cell was on loan from another group who had drilled out the bottom of the gas chamber and replaced it with a new base plate. This was done in order to minimise the working distance for use in an inverted setup.

In this configuration, activation, line purging, experimentation with methanol and line purging were conducted in sequence, extending the total run-time of the experiments. Proposed amendments to this set up for future experimentation are included in Section 7. Methanol was introduced into the system by switching a vaporising syringe pump on and off. All products coming out of the reaction cell were sampled in a mass spectrometer before being directed to the exhaust vent.

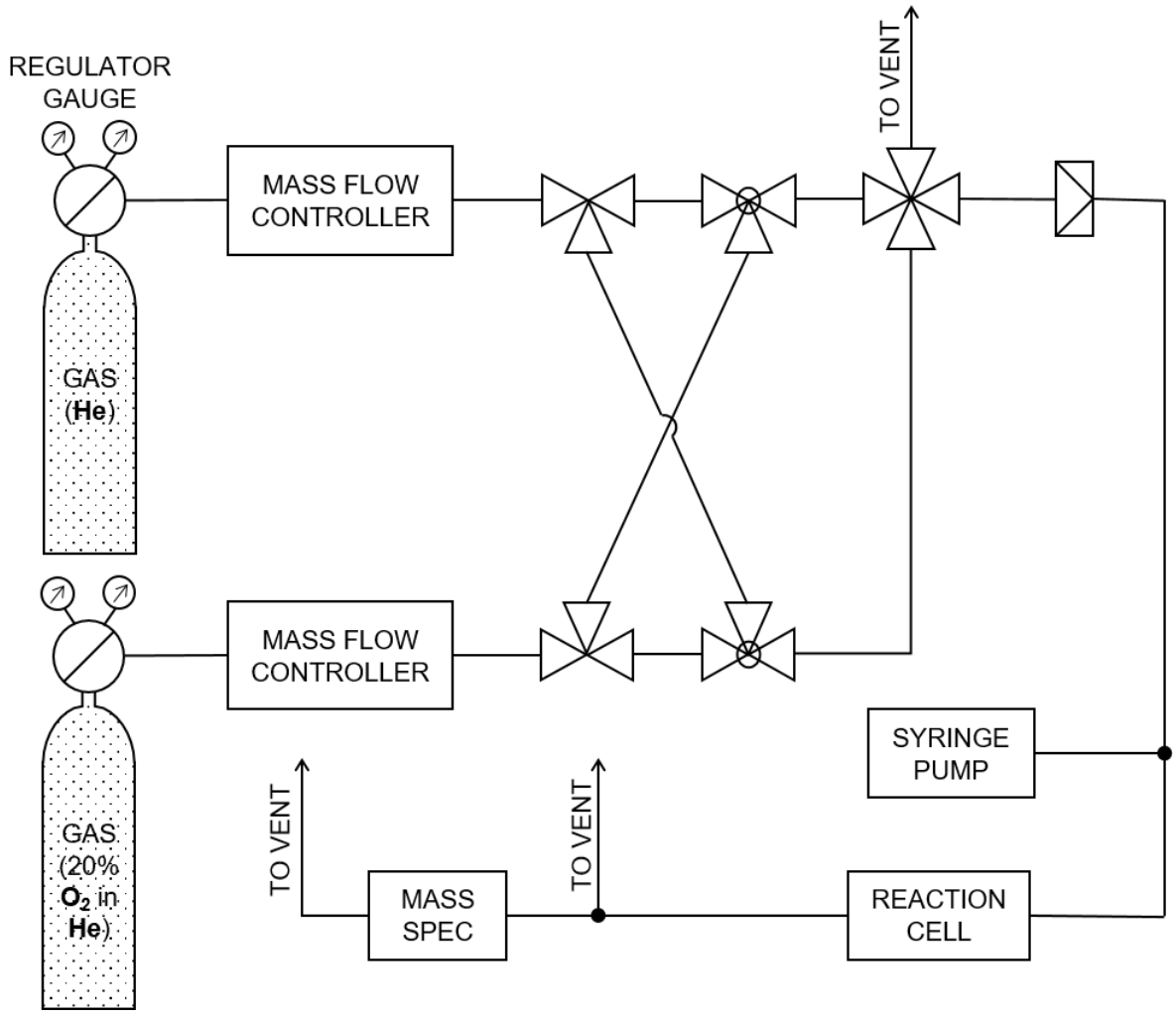

Figure 22 Final setup used featuring a simplified gas lines.

5.3 Method

5 mg[vi] of unreacted H-SSZ-13 were loaded onto a coverslip, which was then placed into the reaction cell. The reaction cell was then mounted onto the microscope stage inside the enclosure and connected to the gas lines and water cooled tubing. Lines were first briefly purged with He gas before oxygen gas flow was started at a rate of 6 mL/min and the temperature of the cell was increased to 550°C in order to activate the sample. Activation was carried out for 2 hours.

After activation, oxygen flow was stopped and the temperature was reduced to 280°C. Lines were purged with He for 1.5 hours to cleanse all oxygen from the closed system before introducing methanol. At this point[vii], the microscope stage was focused and three separate fields of view were selected, recording their x-y co-ordinates. Methanol injection is begun at a rate of around 0.4 µL/min. FLIM images are collected at 5 minute intervals, cycling through the three fields of view. Mass spec data is monitored until products stabilise to determine when the reaction is completed. Once the reaction is completed, methanol is switched off and lines are purged with He as the temperature is cooled to room temperature.

5.4 In-situ Results

Figure 23 and Figure 24 show two fields of view of the catalyst at different times. t_{meth} represents the time elapsed since starting methanol injection. At the beginning of the run, it can be seen that fluorescent lifetimes are long, with a distribution peak at around 5 ns. By 50 minutes, lifetimes across the sample have shifted dramatically to a shorter average lifetime of around 950 ps.

[vi] Such a low volume of sample was selected due to the small size of the coverslip, and the low gas flow rates being used within the cell, which limited the total amount of methanol that could be delivered to the sample within a reasonable period of time.

[vii] Microscope stage is focused after the temperature has been dropped to the final reaction temperature for methanol, as the temperature change from 550°C to 280°C causes the sample to drift.

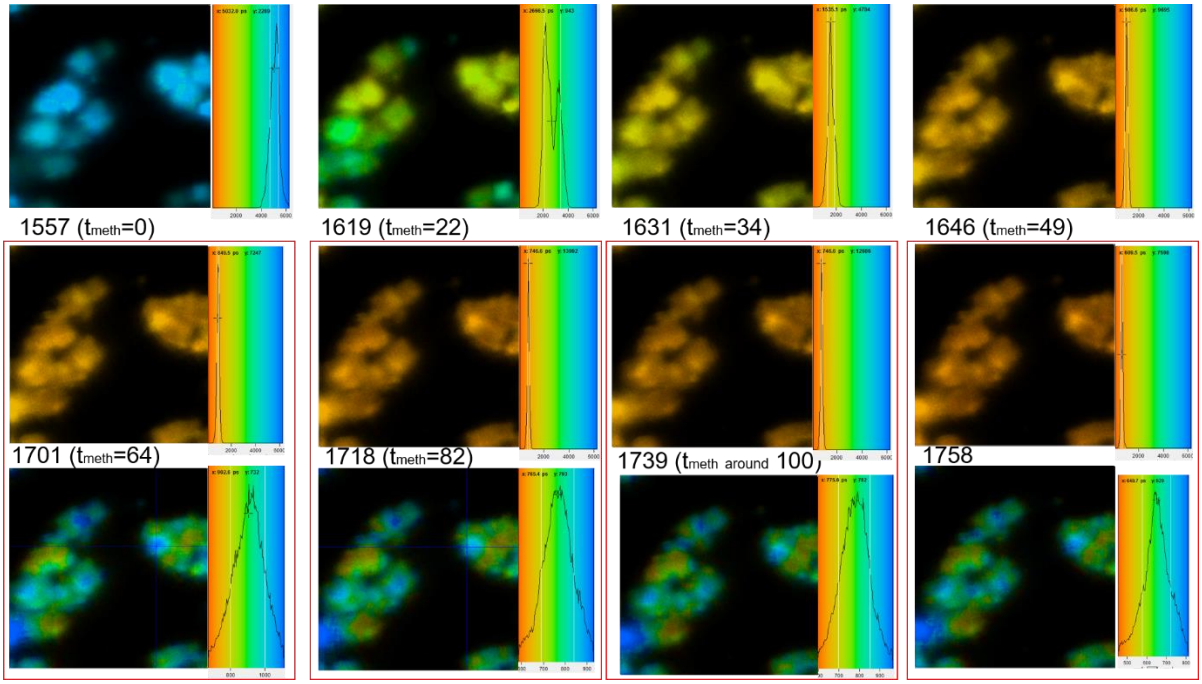

Figure 23 In situ images of position one of a field of view of H-SSZ-13 reacted under vaporised methanol at 280℃ depicting a change in lifetimes from longer lived to short lifetimes

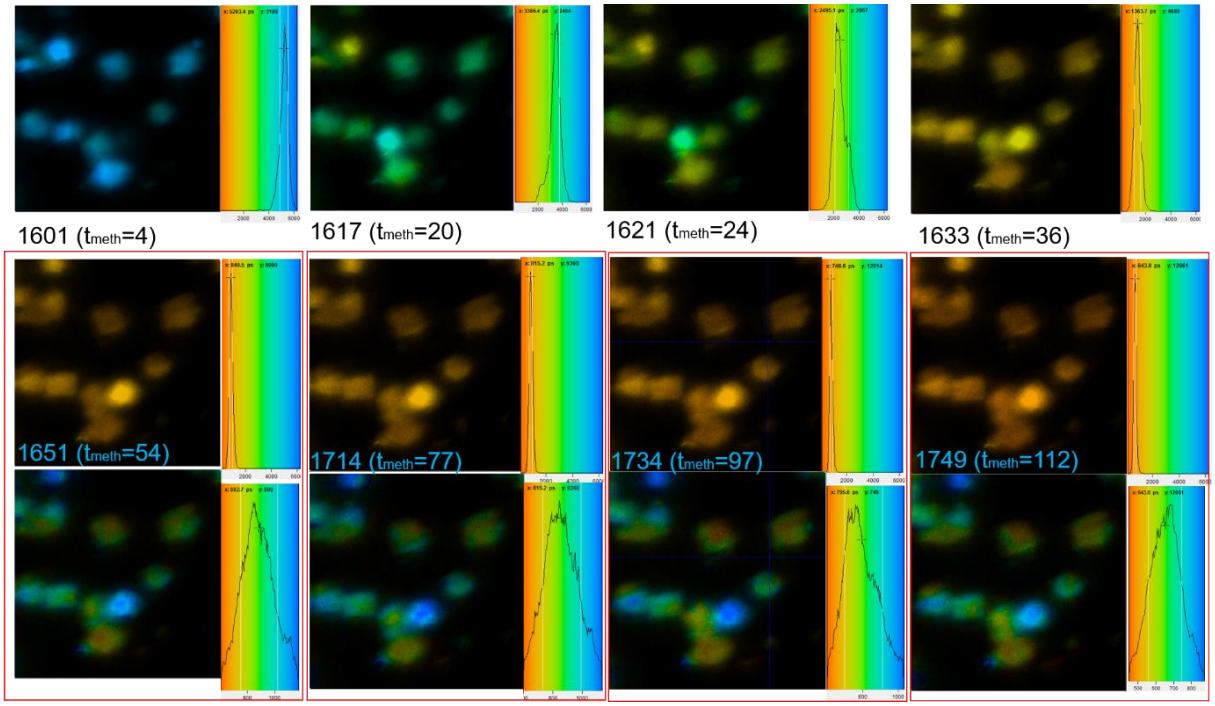

Figure 24 In situ images of position two of a field of view of H-SSZ-13 reacted under vaporised methanol at 280℃ depicting a change in lifetimes from longer lived to short lifetimes

5.5 Ex-situ Results

Further imaging of the same samples was conducted using a different objective lens. A Nikon x60 Plan Apochromat water immersion lens was selected for its higher resolution. A distribution of lifetimes from around 100 to 300 ps were observed.

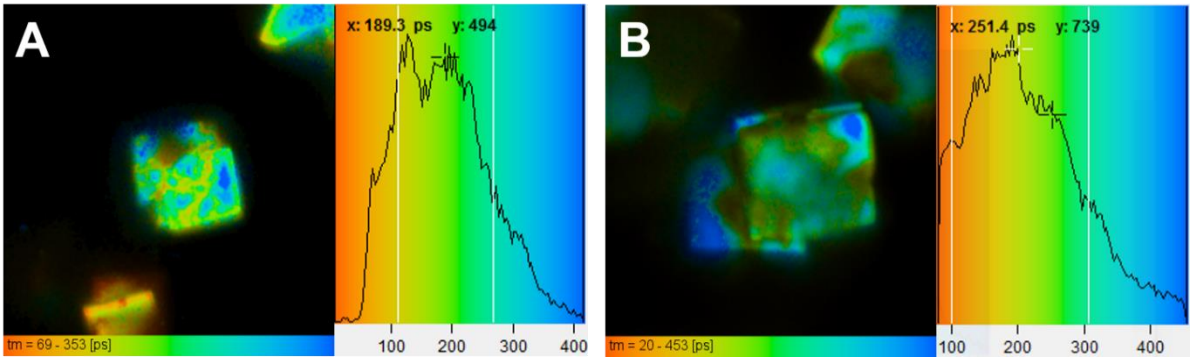

Figure 25 Lifetimes across ex situ crystals of reacted H-SSZ-13

A noticeable resolution enhancement can be observed in the comparison of images in Figure 24 and Figure 25. Where in Figure 25, the sharp edges of the cuboidal H-SSZ-13 crystals are clearly visible, in Figure 24 the same crystals appear much more blurred. This is a significant consideration if the quantitative analysis of lifetime variation across a crystal is important, as the images generated in Figure 24 provide less region specific information than those taken with the x60 Nikon water immersion lens in Figure 25. This highlights the need for a reaction cell that can accommodate a better lens[viii], as long working distance objective lenses have a notoriously compromised numerical aperture.

[viii] Meditating briefly on a point raised in Section 2.2 discussing the challenges of deconvoluting non-radiative pathways, it follows that the accurate and meaningful interpretation of quantitative fluorescent lifetime images rests heavily on the quality of images obtained. As such, an ongoing effort will be made in future iterations of the experiment to optimise all facets of the microscopic setup.

6 Preliminary Spectral-FLIM Imaging

It is intended in future experiments to repeat the experiment performed in Section 6 with a spectral-FLIM setup. Spectral data will introduce the possibility to gain more pointed chemical speciation information, adding a new dimension of catalytic relevance to images collected from this configuration. The following data set has been presented as a short case study to highlight the value this technique can bring.

Case Study: Using spectral detection to highlight local variations in chemical composition across a bulk sample

6.1 Sample Background

98% purity benz[b]anthracene ($C_{18}H_{12}$) was purchased from Sigma-Aldrich as a reference sample for a potential product formed in the MTO reaction.

6.2 Experimental Setup

As in Section 5.2.1 a Nikon microscope body with a Becker & Hickl HPM-100-40 high detector and 80 MHz 405 nm pulsed single photon excitation laser source was used. A Nikon x60 Plan Apo water immersion lens was used. The spectral detector used was a modular HR2000CG-UV-NIR from Ocean Optics. Spectra were collected using a laser power of approximately 15 µW and an integration time of 5000 milliseconds.

6.3 Method

8 different emission spectra were obtained by parking the laser beam at 8 different points across a field of view of the sample as shown in Figure 26. In particular, regions appearing to show a different lifetime were selected.

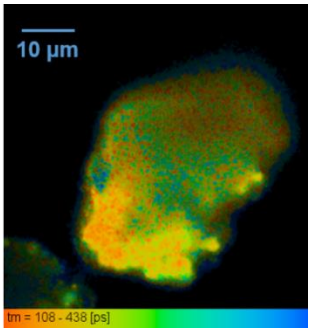

Figure 26 FLIM image of benz[b]anthracene

6.4 Results

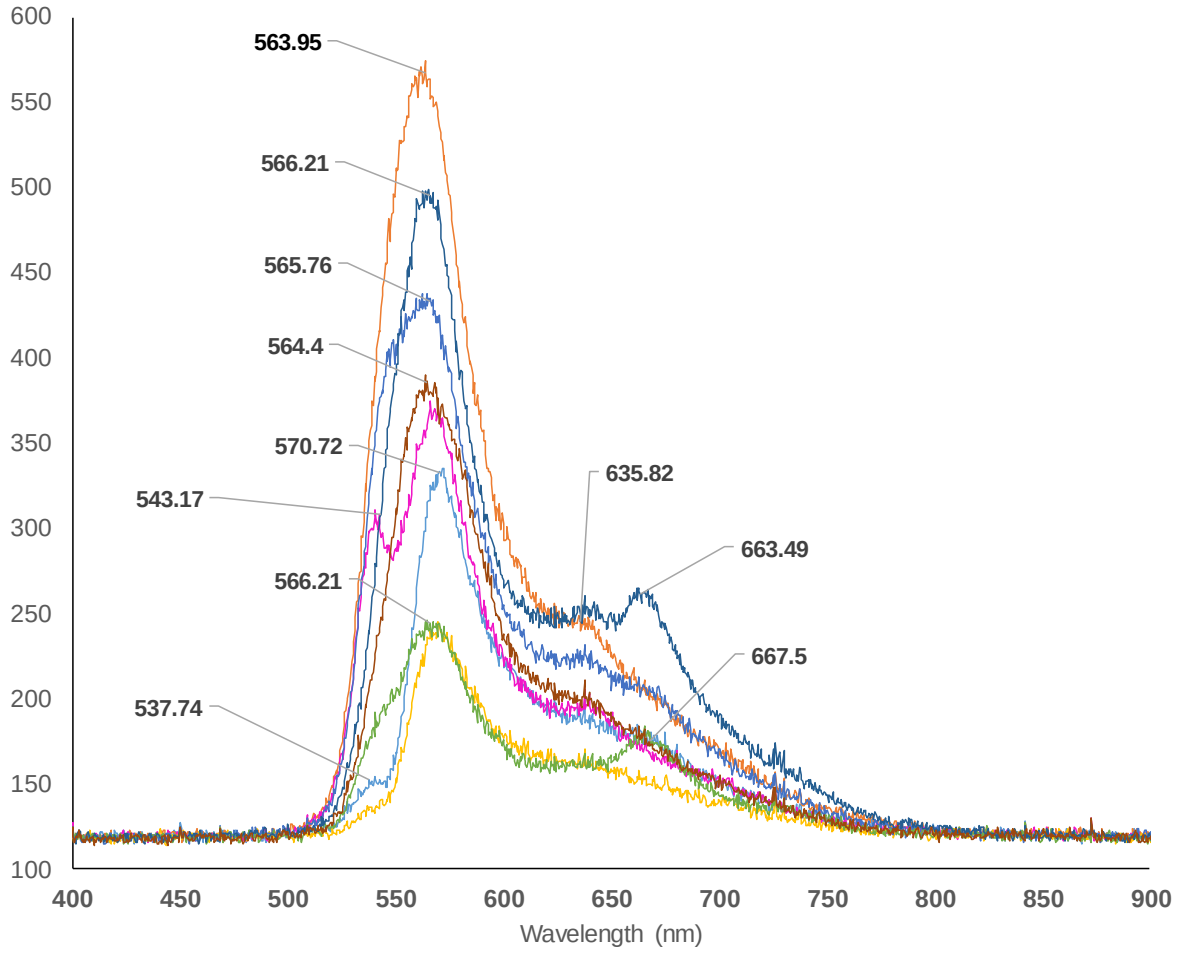

Figure 27 Emission spectra with 405 nm excitation recorded at different points across a powder distribution of factory standard benz[b]anthracene

Figure 27 shows emission spectra with slightly different shapes. In all instances, the prominent peak at 565 nm is visible, although appears slightly shifted to 570 nm in a couple of instances. Beyond this the variation in the spectra is greater. At least 3 of the 8 spectra appear to show a shoulder on the main peak at around 540 nm. 2 of the 8 spectra show a visible second peak at 665 nm. Finally, a subtle shoulder can be seen at least 4 of 8 spectra at about 635 nm.

As can be seen by the scale of the image in Figure 26, the variations in spectra being recorded are being observed over distances of no greater than 20-30 µm across, showing that the technique is capable of discriminating more subtle differences over a more sensitive length scale.

The differing peak positions and trace shape could be explained by inhomogeneities in composition across the sample. If so, the 2% of impurities is very evident when analysed with this method. Large differences in intensity of the traces may also be attributed to local

differences in concentration or differences in the focal plane. Also if the sampling volume is different, for example if only the edge of the sample is being illuminated, a lower overall intensity in the trace might be observed.

7 Future Work

A timetable for future work focusing on the first six months of 2017 is included in Figure 28. For the third and fourth years of the project, there may be a return to exploration of super-resolution for nanomaterials, a view to attempt correlative electron microscopy or the integration of Kerr-gate Raman into a FLIM microscope.

Month	Jan		Feb		Mar		Apr		May		Jun		Jul	Aug	Sep	Oct	Nov	Dec
Week	1-2	3-4	1-2	3-4	1-2	3-4	1-2	3-4	1-2	3-4	1-2	3-4	1-4	1-4	1-4	1-4	1-4	1-4
Beamtime Experiments																		
1. Submit Beamtime Application																		
2. Preparing/Purchasing Components for Beamtime											Depending on scheduling							
3. Scheduled Beamtime											Expected in this period							
4.Outstanding OCTOPUS and new ULTRA Beamtime			OCT						ULT									
Creating a New Reaction Cell																		
1. Designing Reaction Cell																		
2. Building Reaction Cell																		
3. Characterising Reaction Cell																		
Conferences																		
1. Johnson Matthey Conference Flash Talk Prep																		
2. Research Conferences to Attend																		
Additional Experimentation (TBC)																		

Figure 28 Proposed timetable for future work

A beamtime application will be submitted for the June-December round of Central Laser Facility OCTOPUS microscopy usage for an in-situ experiment. In the proposal, a new capillary temperature reaction cell will be mounted onto an inverted microscope stage. The microscope will be configured to provide spectral-FLIM measurements at a series of wavelengths. The ability to obtain in-situ emission spectra by parking the beam at particular points across the sample will be a crucial step in identifying chemical speciation. It is known that emissive hydrocarbons may form within the cage-like structure of the zeolite. As they are trapped inside the framework, such species would not appear on mass spec readings, meaning that changes in emission spectra will provide high impact, in-situ information of carbon species.

Compared to the initial iteration of this in-situ experiment, the following major revisions to the experimental setup will be made:

1. *Different Excitation Wavelengths*

Previously a wavelength of 405 nm was selected, so that FLIM data obtained could be paired with data obtained from a separate Kerr-gated Raman experiment. However, it is likely that while 405 nm is sufficient to probe the zeolite framework, this wavelength is too long to excite some of the hydrocarbons expected to be forming based on literature (e.g. anthracene, pentacene etc.). The next proposal seeks to probe further into the UV, to obtain better excitation

of aromatic hydrocarbon species. It is hoped that measurements will be performed with multiphoton excitation at 600 nm, and to access single photon UV laser excitation by frequency tripling an OPO laser.

2. *New Reaction Cell*

A significant portion of future work planned in the next six months is the design and manufacture of a catalytic reaction cell. Commercial Linkam cells used in previous experiments presented a particular set of problems, including a large dead volume, line connections prone to blockages, and a long working distance in an inverted configuration. It was decided that more catalytically relevant data could be obtained if a tailor made reaction cell were to be engineered. A preliminary design is included below in Figure 29.

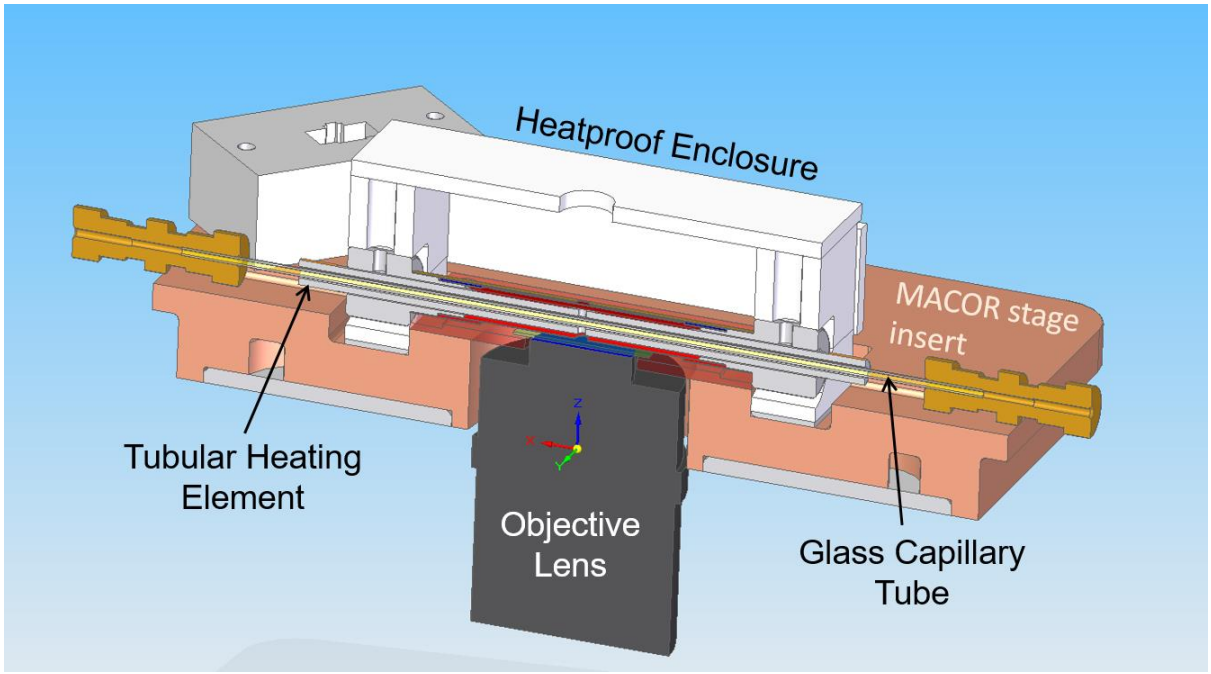

Figure 29 Preliminary design for a customised reaction cell for use in an inverted microscope

Specific benefits of the new cell design are:

- Reduced dead volume with the use of a capillary design, which will increase the efficiency of the catalytic reaction
- Minimised working distance, enabling the use of a better objective lens, increasing the resolution of images obtained

3. *New Gas Schematic*

A major logistical hindrance of the previous setup was the amount of time required to purge lines. As seen in Figure 22, in the original experimental setup one bottle of helium gas

was used as both a purge gas and carrier gas for the methanol, and a separate bottle of oxygen was used to activate the system. In the configuration used the process of purging, activating, purging, and injecting methanol could take over 6 hours as it had to be performed in succession. In the new setup, as shown in Figure 30, an additional helium bottle will be included such that purging and methanol injection can happen via independent lines. This will significantly reduce the reaction times allowing twice as many experiments to be carried out during the beam-time run.

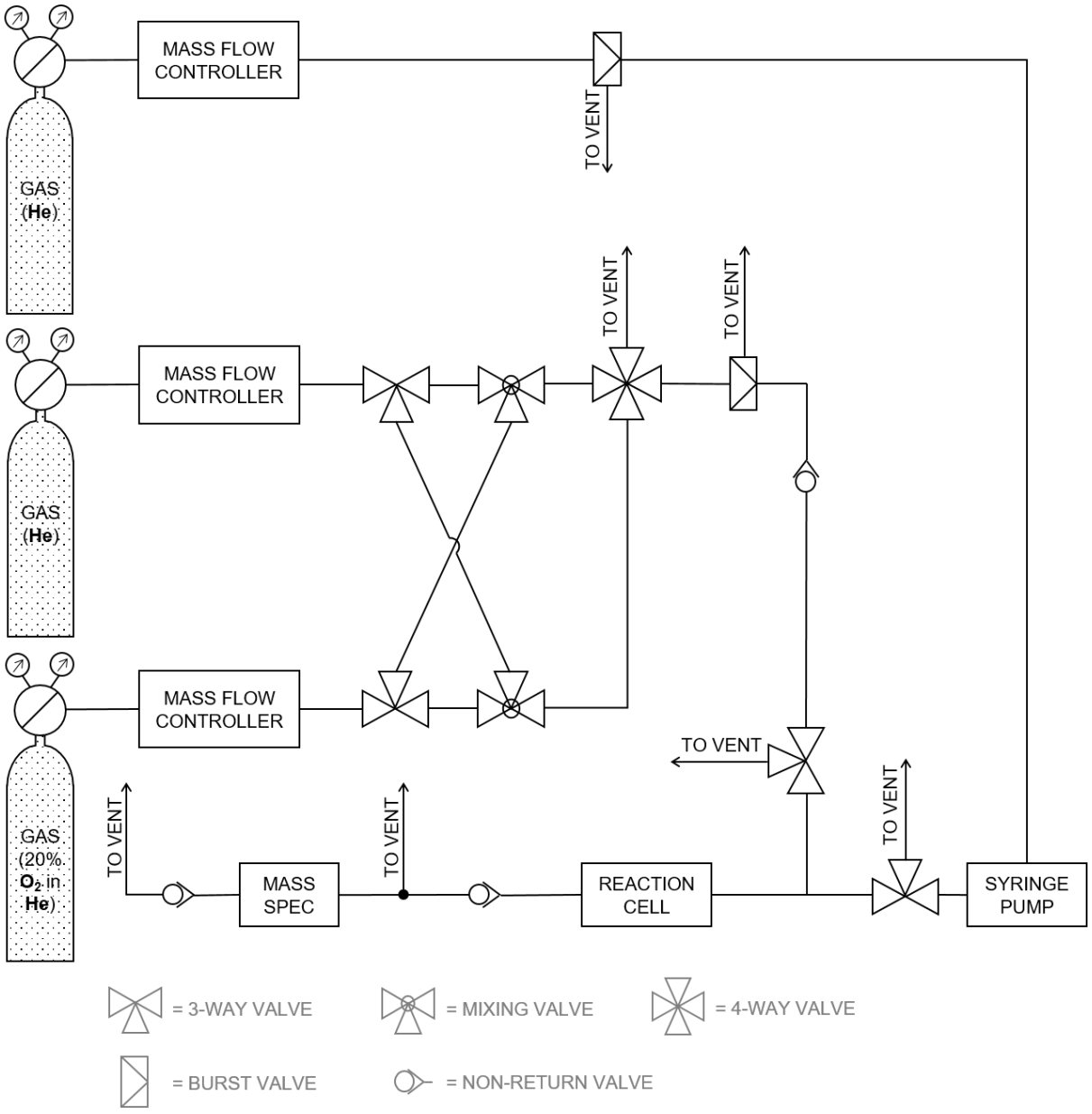

Figure 30 Proposed revisions to gas schematic to include a more efficient valve design and the addition of another He tube to increase the rate at which experiments can be performed.

References

1. Colin Cundy, P. C. The hydrothermal synthesis of zeoliltes: history and development from the earliest days to the present time. *Chem. Rev*. **103,** 663–702 (2003).

2. Kubarev, A. V., Janssen, K. P. F. & Roeffaers, M. B. J. Noninvasive Nanoscopy Uncovers the Impact of the Hierarchical Porous Structure on the Catalytic Activity of Single Dealuminated Mordenite Crystals. *ChemCatChem* **7,** 3646–3650 (2015).

3. Janssen, K. P. F. *et al.* Chem Soc Rev Single molecule methods for the study of catalysis : from enzymes to heterogeneous catalysts. 990–1006 (2014). doi:10.1039/c3cs60245a

4. Gion Calzaferri, Arantzazu Zabala Ruiz, Huanrong Li, Stefan Huber, A. D. Organising supramolecular functional dye-zeolite crystals. *Acta Crystallogr.* **A62,** s71 (2006).

5. Calzaferri, G., Huber, S., Maas, H. & Minkowski, C. Host – Guest Antenna Materials Angewandte. 3732–3758 (2003). doi:10.1002/anie.200300570

6. Roeffaers, M. B. J. *et al.* Spatially resolved observation of crystal-face- dependent catalysis by single turnover counting. **439,** 1–4 (2006).

7. Roeffaers, M. B. J. *et al.* Fluorescence microscopy : Bridging the phase gap in catalysis. **126,** 44–53 (2007).

8. Roeffaers, M. B. J. *et al.* Super-resolution reactivity mapping of nanostructured catalyst particles. *Angew. Chemie - Int. Ed.* **48,** 9285–9289 (2009).

9. Kerssens, M. M. *et al.* High-Resolution Single-Molecule Fluorescence Imaging of Zeolite Aggregates within Real-Life Fluid Catalytic Cracking Particles **. 1836–1840 (2015). doi:10.1002/anie.201410236

10. Luis Aramburo, Javier Ruiz-Martinez, Jan Hofmann, B. W. Imaging the effect of a hydrothermal treatment on the pore accessibility and acidity of large ZSM-5 zeolite crystals by selective staining. *Catal. Sci. Technol.* **3,** 1208–1214 (2013).

11. Karwacki, L., Stavitski, E., Kox, M. H. F., Kornatowski, J. & Weckhuysen, B. M. Intergrowth Structure of Zeolite Crystals as Determined by Optical and Fluorescence Microscopy of the Template-Removal Process **. 7228–7231 (2007).

doi:10.1002/anie.200702012

12. Qi, G., Xie, Z., Yang, W., Zhong, S. & Liu, H. Behaviors of coke deposition on SAPO-34 catalyst during methanol conversion to light olefins. **88,** 437–441 (2007).

13. Chung, Y., Mores, D. & Weckhuysen, B. M. Applied Catalysis A : General Spatial and temporal mapping of coke formation during paraffin and olefin aromatization in individual H-ZSM-5 crystals. *"Applied Catal. A, Gen.* **404,** 12–20 (2011).

14. Nordvang, E. C., Borodina, E., Ruiz-martínez, J., Fehrmann, R. & Weckhuysen, B. M. Effects of Coke Deposits on the Catalytic Performance of Large Zeolite H-ZSM-5 Crystals during Alcohol-to-Hydrocarbon Reactions as Investigated by a Combination of Optical Spectroscopy and Microscopy. 17324–17335 (2015). doi:10.1002/chem.201503136

15. Qi, H. Fluorescence imaging technology (FI) for high-throughput screening of selenide-modified nano-TiO2 catalysts. *Chem. Commun.* **52,** 2944–2947 (2016).

16. Matousek, P. *et al.* Fluorescence suppression in resonance Raman spectroscopy using a high-performance picosecond Kerr gate. 983–988 (2001).